Risk-Based Optimal Design of Seismic Protective Devices for a Multi-component Bridge System Using Parameterized Annual Repair Cost Ratio

Chunxiao Ning

Department of Civil Engineering

McGill University, Montreal

June 2022

A thesis submitted to McGill University in partial fulfillment of the requirements of the degree of Master of Engineering.

Abstract

Base isolators and fluid viscous dampers are viable protective devices that have been commonly considered in the seismic protection of civil engineering structures. However, the optimal design of these devices remains a tedious and iterative undertaking due to the uncertainty of ground motions, the nonlinear behavior of the structure, and its change of dynamic characteristics (i.e., effective stiffness and damping ratio) under each new design. The optimal design problem becomes more challenging concerning a multi-response bridge system where conflicting damage potential are often expected among multiple bridge components (e.g., column, bearing, shear key, deck unseating, foundation). In this respect, this study develops a risk-based optimization strategy that directly links the expected annual repair cost ratio (ARCR) of the bridge to the design parameters of base isolators and fluid dampers. This strategy is achieved by devising a multi-step workflow that integrates a seismic hazard model, an experimental design of bearings and dampers, nonlinear time history analysis (NLTHA) of multi-component bridge models, a logistic regression towards parameterized component-level fragility models, and a bridge system-level seismic loss assessment. The developed ARCR is parameterized as a convex function of the influential parameters of seismic protective devices. As such, optimal bearing and damper designs can be pinpointed by directly visualizing the global minimum of the parameterized ARCR surface. The optimal design is carried out against a typical reinforced concrete highway bridge in California that is installed with the fluid dampers and three types of widely-used isolation bearings – the elastomeric bearing, lead-rubber bearing, and friction pendulum system. It is shown that optimal design parameters can be obtained to significantly reduce the expected ARCR of the bridge, whereas combining optimally designed bearings and dampers can provide the minimum seismic

risk. In addition, the robustness of the optimization framework is verified by carrying out the sensitivity analysis, and it is shown that the capacity model, damage ratio and replacement cost for column and deck unseating constitute the major parts of uncertainty in the analysis.

Résumé

L'isolateur de fondation et l'amortisseur visqueux liquide sont des dispositifs de protection couramment utilisés dans les structures de génie civil. Cependant, en raison de l'incertitude du mouvement du sol, du comportement non linéaire de la structure et de la variation de ses caractéristiques dynamiques (c. - à - D. rigidité effective et rapport d'amortissement) dans chaque nouvelle conception, la conception optimale de ces dispositifs reste une tâche itérative fastidieuse. La question de l'optimisation de la conception devient plus difficile pour les systèmes de ponts à réponses multiples, car il y a souvent des possibilités conflictuelles de dommages entre plusieurs éléments de pont (p. ex., colonnes, roulements, clés de cisaillement, vides de pont, fondations). À cet égard, l'étude a mis au point une stratégie d'optimisation fondée sur les risques qui établit un lien direct entre le rapport des coûts d'entretien annuels prévus (RC) des ponts et les paramètres de conception des isolateurs de fondation et des amortisseurs de fluides. La stratégie est mise en œuvre en concevant un flux de travail en plusieurs étapes qui intègre le modèle de risque sismique, la conception expérimentale des roulements et des amortisseurs, la régression logique vers le modèle paramétrique de vulnérabilité au niveau des composants et l'évaluation des pertes sismiques au niveau du système de pont. L'arcr développé est paramétré en fonction convexe des paramètres d'influence du dispositif de protection contre les tremblements de terre. Par conséquent, la meilleure conception du roulement et de l'amortisseur peut être déterminée avec précision en visualisant directement la valeur minimale globale de la surface paramétrique de l'arc. Une conception optimisée a été réalisée pour un pont routier typique en béton armé en Californie, qui est équipé d'amortisseurs de fluide et de trois types de supports d'isolation sismique largement utilisés - des supports élastiques, des supports en caoutchouc plomb et des systèmes de pendules à friction. Les résultats montrent que les paramètres de conception optimaux peuvent être obtenus pour réduire considérablement l'arc attendu du pont, tandis que les roulements et les amortisseurs combinés à une conception optimisée peuvent fournir un risque sismique minimal. De plus, la robustesse du cadre optimisé est vérifiée par l'analyse de sensibilité. Les résultats montrent que le modèle de capacité portante, le taux de dommages et le coût de remplacement de la colonne et du pont vides constituent les principales incertitudes de l'analyse.

Acknowledgements

This study is finished under the guidance of my supervisor, Prof. Yazhou Xie, and I would like to express my sincere appreciation to him for continuously giving me advice, encouragement, support, and inspiration. Prof. Xie led me on the road of research step-by-step. He patiently helps me sort out every technical detail and revise my writings, word by word. He shares many valuable research experiences with me and encourages me to stay calm and rigorous when doing research. These instructions and accompanying have a significant influence on my later academic life.

I am thankful to my friends and families for their encouragement and accompany. During the period of the COVID pandemic, I spent a lot of time with my mother and grandmother, and I thank them for their unconditional support and comfort. I would like to thank my friends, as they are always there when I feel isolated, and they are glad to listen to me.

I am also thankful to JJ Lin and Sodagreen for their music, which gives me hope when I feel depressed, and teaches me how to face pain and suffering. I also appreciate everyone who gives dedicated service to make the world a better place. Finally, I would like to thank myself for my persistence and effort.

Contribution of Authors

This thesis has been written following the requirements of Graduate and Postdoctoral Studies for a manuscript-based thesis. The main findings of the research undertaken by the author as part of his master's program are presented in a single manuscript. The author carried out the numerical analysis and wrote the manuscript under the supervision of Prof. Yazhou Xie (supervisor). The publication detail is presented below:

- Ning, C. and Xie, Y., 2022. Risk-Based Optimal Design of Seismic Protective Devices for a Multicomponent Bridge System Using Parameterized Annual Repair Cost Ratio. Journal of Structural Engineering, 148(5), p.04022044.

Contents

List of Figures

List of Tables

Chapter 1 – Introduction

1.1 Problem description and motivation

Highway bridges are one of the most vulnerable components in transportation networks under seismic hazards, and their failure brings multiple longstanding socioeconomic impacts to the affected regions, such as casualties, economic losses, and downtime of regional traffic (Bruneau, Wilson and Tremblay, 1996; Basöz *et al.*, 1999). The state of California has a complex transportation system, and over half of the highway bridges are constructed before 1971 (FHWA, 2021). Those early-designed bridges are more prone to seismic damage due to the lack of seismic design. In addition, California state features high seismicity, influenced by the active San Andreas fault that forms the boundary between the pacific plate and the North American plate. The high seismic hazard and dense infrastructures result in severe seismic loss and risk, as witnessed by historical earthquake events. According to the report from Caltrans, the Northridge earthquake damaged 233 bridges among 850 inspections in Southern California (Caltrans, 1994), and more than 67% of the damaged bridges were designed before the 1970s. Besides, other earthquakes [e.g., the 1971 San Fernando earthquake (Mitchell *et al.*, 1995) and the 1989 Loma Prieta earthquake (Mitchell, Tinawi and Sexsmith, 1991)] revealed that early designed bridges exhibited common failure modes, such as 1) non-ductile failure of columns due to inadequate reinforcement; 2) deck unseating due to the narrow seat width; 3) large movement of foundations on soft soil.

Since 1971, the state of California has introduced extensive retrofitting projects to improve the seismic resistance of bridges. For example, the restrainer is installed between the deck and abutment to constrain span unseating, and columns are coated with steel jackets to improve the ductility and shear strength (Mitchell *et al.*, 1995). The Northridge earthquake verified the effectiveness of those seismic retrofitting measurements, as most retrofitted bridges sustained only minor damages (Basöz *et al.*, 1999).

In addition to the aforementioned traditional retrofitting schemes, the installation of supplemental seismic protective devices (e.g., isolation bearings and fluid viscous dampers) shows promise in mitigating the seismic risk of bridges (Gidaris and Taflanidis, 2015; Xie and Zhang, 2017, 2018). These devices feature excellent energy dissipation ability, and a considerable part of the seismic energy is dissipated through their hysteretic mechanisms. To be specific, isolation bearing can be regarded as a “soft connecter” between superstructure and substructure. It lengthens the natural period of the bridge, and its yielding strength limits the force transmitted to the substructure. In contrast, fluid viscous dampers supply additional damping into the structure system. They usually are installed to connect the deck to abutments and/or columns. A large amount of energy can be dissipated through fluid dampers under earthquakes. At the same time, they constrain the relative movement between superstructure and substructure, which effectively avoids bearing failure and deck unseating (Park *et al.*, 2004; Ghosh, Singh and Thakkar, 2011; Karalar, Padgett and Dicleli, 2012). Compared to traditional retrofitting methods, seismic protective devices also provide the structure system with additional energy dissipation, such that the inelastic damage of the main structure is effectively reduced.

The effectiveness of seismic protective devices depends on multiple factors, including the dynamic property of the main structure, the mechanical parameters of the devices, and the characteristics of seismic hazards. The design of seismic protective devices requires a thorough understanding of the complex nonlinear interaction between those factors (Symans *et al.*, 2008). In this regard, the state of research can be generally classified into deterministic and probabilistic approaches. The deterministic method neglects the variability in each of these factors, and the seismic performance of retrofitted bridges has been analyzed using design spectra or a handful of earthquake ground motions (Wang, Chung and Liao, 1998; Makris and Zhang, 2004a; Jangid, 2005; Soneji and Jangid, 2007; Ozbulut and Hurlebaus, 2011a). Based on individual analyses, these prescriptive approaches elucidate the dynamic interplay between the seismic protective device and the main structure. However, their drawback is obvious: the seismic hazard is represented by a small number of selected ground motions, and the uncertainties cannot be faithfully captured. In contrast, the probabilistic approach explicitly quantifies and propagates uncertainties in seismic hazard, structural demand, seismic capacity, and exposure information (Gardoni, Mosalam and Kiureghian, 2003).

The performance-based earthquake engineering (PBEE) framework proposed by the Pacific Earthquake Research Center (PEER) has offered a feasible pathway to conduct the design and optimization of seismic protective devices in a fully probabilistic manner (Cornell and Krawinkler, 2000). PBEE stands on the premise that seismic risk can be predicted and evaluated with quantifiable confidence in all pertinent uncertainties that propagate from earthquake occurrence modelling to the assessment of earthquake consequences, such as casualties, dollar losses, and downtime (Porter, Beck and Shaikhutdinov, 2002; Park *et al.*, 2004). The PBEE has also fostered related studies on highway bridges. For instance, recent works have evaluated the effectiveness of isolation devices and other retrofit measures on the seismic fragility of bridges (Li *et al.*, 2020; Xiang and Li, 2020; Montazeri, Ghodrati Amiri and Namiranian, 2021; Wei *et al.*, 2021). These studies have indicated a significant change in the seismic fragility between isolated and non-isolated bridges. However, previous studies on the optimal design of seismic protective devices are computationally demanding. To be specific, Zhang and Huo (2009) used permutations to include all design scenarios and computed the fragility curve for each combination of design parameters, which requires hundreds of nonlinear time history analyses (NLTHA) for each scenario to develop fragility curves. Similarly, Xie and Zhang (2017, 2018) relied on genetic algorithm to identify the optimal design under each ground motion. Hundreds or even thousands sets of computations are needed in these studies. In addition, these studies defined optimization objectives on discrete hazard levels, while the mitigation of the overall seismic risk stays unclear.

To this end, the current study develops a complete risk-based optimization framework that (1) integrates the seismic damage and loss of multiple bridge components; (2) derives a performance objective that is intensity independent; and (3) does not require an iterative process to identify the optimal design. The proposed multi-step workflow engages the parameterized fragility models (Ghosh, Padgett and Dueñas-Osorio, 2013; Kameshwar and Padgett, 2014) into the existing PBEE framework, making the fragility function depending on both intensity measure (*IM*) and design parameters of seismic protective devices. By convolving the seismic hazard model, parameterized fragility model, and bridge exposure information, the system-level expected annual repair cost ratio (ARCR) is derived. The ARCR is shown to be convex with respect to device design parameters, and the optimal design parameters can be directly pinpointed by visualizing the global minimum of the convex ARCR surface. The proposed optimization methodology is used to retrofit a typical early-designed bridge in California, considering six different design scenarios (i.e., three bearing cases, and three bearing plus damper cases). The protection effectiveness of these different bearing and damper cases are also compared.

1.2 Outline of this study

The research is organized into five subsequent chapters with the following contents:

Chapter 2 presents a literature review regarding the development of the PBEE framework and seismic protective devices.

Chapter 3 shows the proposed risk-based optimization framework and its components, including the seismic hazard model, finite element analysis, parameterized fragility model, and expected annual repair cost ratio (ARCR).

Chapter 4 applies the proposed methodology to retrofit an early-designed benchmark bridge using seismic protective devices. The risk mitigation effect of various isolation bearings and viscous dampers is compared, and the sensitivity analysis is also carried out.

Chapter 5 presents the conclusions from the present research.

Chapter 2 – Literature Review

2.1 Performance-based earthquake engineering (PBEE) framework

The conventional earthquake-resistance design relies on the nonlinear behavior of certain structural components to dissipate seismic energy. Such nonlinear behavior is associated with structural damage, such as forming plastic hinges on columns and beams, and cracking and spalling of concrete and masonry structures. Seismic damage to civil engineering structures would induce direct and indirect costs (e.g., closure and rerouting time, and causalities). However, the seismic risk and loss remain difficult to estimate because the conventional design didn't reliably predict seismic damage and consequences (Constantinou *et al.*, 2007).

The Performance-based Earthquake Engineering (PBEE) framework (Cornell and Krawinkler, 2000) bears the potential to replace the existing load-and-resistance-factor design (LRFD) method in design codes (Porter, 2003). The early versions of PBEE methodologies were documented in different reports (e.g., SEAOC's Vision 2000 report (1995), ATC (1996a, 1996b) and FEMA (1997, 2000)) more than 20 years ago. However, these initiatives fall short in quantifying all sources of uncertainties. For instance, the structure's performance is assumed to be deterministic: it is considered acceptable if the demand is below a predefined limit state. Subsequently, the Pacific Earthquake Engineering Research (PEER) Center updated its PBEE framework to assess the system-level performance of the structure in a probabilistic manner. The PBEE framework is mainly composed of the following probabilistic elements: seismic hazard model, demand and capacity model, fragility model, and exposure model. These four elements are analyzed through the corresponding four stages: hazard analysis, structural analysis, damage analysis, and loss analysis (Günay and Mosalam, 2013), as shown in Figure 2.1. Different stages

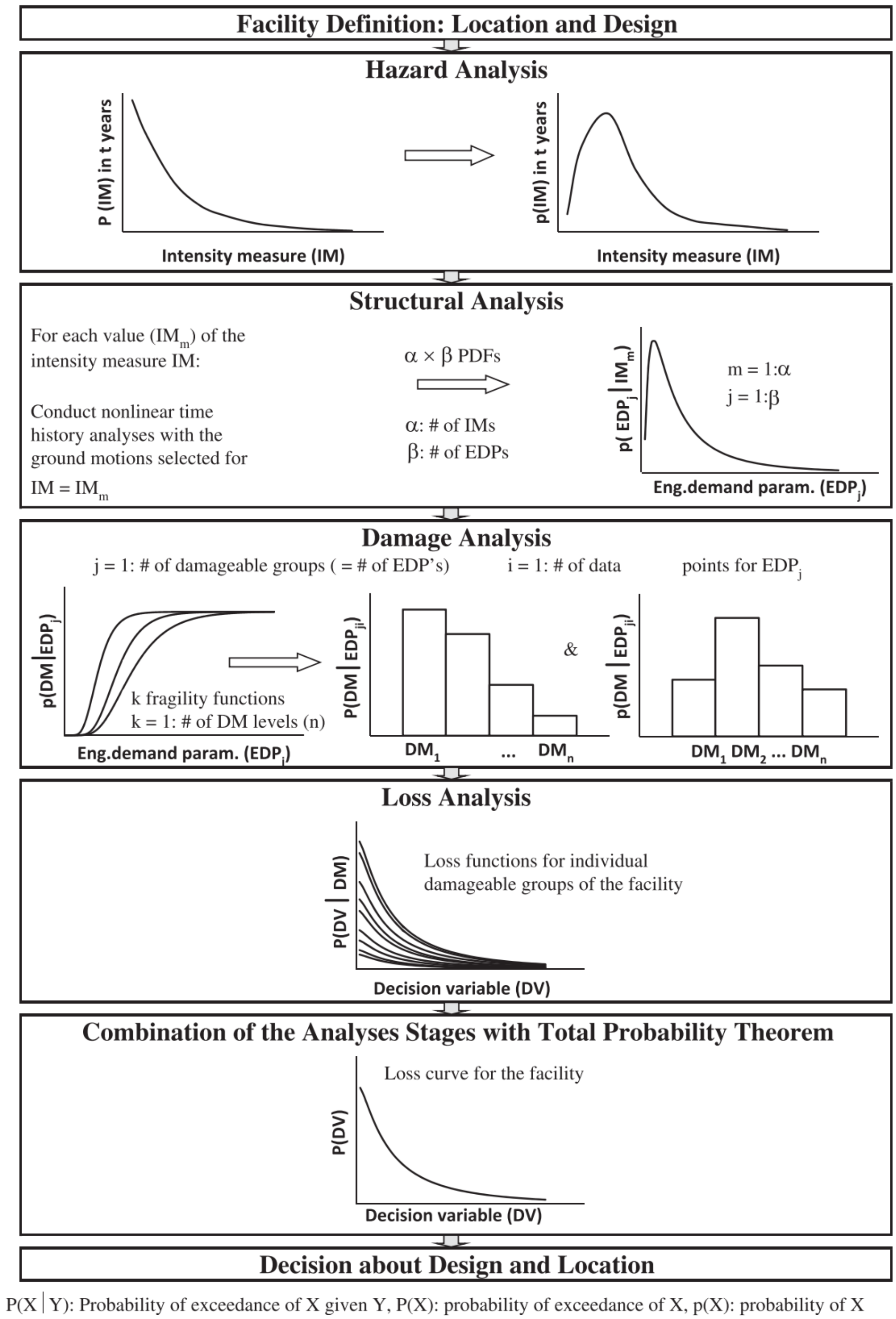

Figure 2.1 PEER PBEE analysis stages (Günay and Mosalam, 2013)

are represented by probabilistic distribution functions conditioning only on the previous adjunct stage, known as a discrete Markov process (Moehle and Deierlein, 2004). The PEER's PBEE framework can be represented by combining these distribution functions using the total probability formula, as shown in Eq. (2.1).

$$\lambda(DV) = \int\int\int P(DV|DM)dP(DM|EDP)dP(EDP|IM)d\lambda(IM|O,D) \tag{2.1}$$

where λ(·) denotes the mean annual rate of exceedance, P(·) is the complementary cumulative distribution function, *DV* is the decision variable, *DM* stands for the structural measure, *EDP* denotes the engineering demand parameter, and *IM* denotes the ground motion intensity measure. Under the conditional independence assumption, the PEER formulation allows seismic risk assessment to be decomposed into multiple individual modules, where different sources of uncertainties from each module can be quantified and propagated.

Many studies have leveraged the PBEE framework to assess the seismic performance of buildings (Ramamoorthy, Gardoni and Bracci, 2006; Tesfamariam and Goda, 2015; Gur, Xie and DesRoches, 2019) and bridges (Floren and Mohammadi, 2001; Moehle and Deierlein, 2004; Mackie and Stojadinović, 2007; Mangalathu, 2017; Yoon *et al.*, 2019). Mangalathu et al. (2016, 2017) grouped bridges in California into classes according to their design and structural performance, and studied the seismic fragility of each group of bridges. Similarly, Padgett et al. (2008) developed fragility curves for retrofitted bridges using the analytical method. Kameshwar et al. (2014) analyzed the annual risk of the bridge under the action of earthquake and flood, and the PBEE framework is used to estimate the failure probability under different hazards. Goda and co-authors analyzed the seismic loss of reinforced concrete frame buildings (Tesfamariam and Goda, 2015; Goda and Tesfamariam, 2019) and wood frame buildings (Goda and Atkinson, 2011)) in Canada, taking into consideration the different earthquake types across the country. These studies have shown that the PBEE framework enables reliable estimations of seismic fragility and risk of civil engineering structures. However, the research on PBEE-based optimization design is still lacking consistency. This thesis fills this knowledge gap by developing a framework that gives the optimal design scenario without iterative and tedious computations.

2.2 Seismic protection techniques of bridges

In the last three decades, seismic protective devices have been developed to mitigate the seismic effect on highway bridges. These devices improve the seismic performance of bridges by 1) supplementing additional damping to the system; 2) elongating the natural period of the structure (Xie and Zhang, 2017); 3) redistributing the force between superstructures and substructures (Constantinou *et al.*, 2007). In particular, seismic protective devices (e.g., bearings, dampers, and restrainers) require certain relative movement/velocity to fully engage during seismic shaking. Thus, they are commonly installed between the deck and columns/abutments for highway bridges, as shown in Figure 2.2.

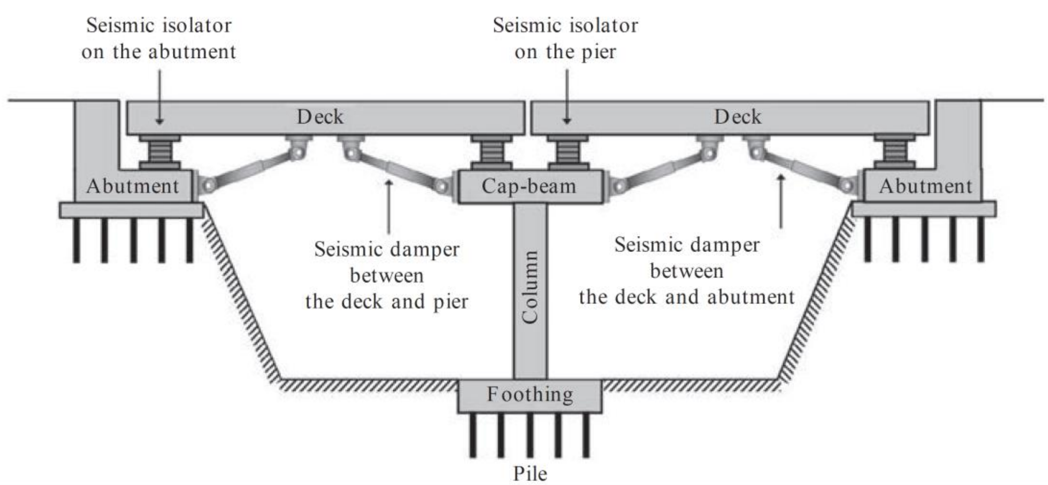

Figure 2.2. Typical configuration of seismic protective devices (Agrawal and Amjadian, 2022)

2.2.1 Isolation bearings

Isolation bearings are well-accepted seismic protective devices. Many researchers have investigated their seismic applications in both newly-designed and retrofitted bridges (Makris and

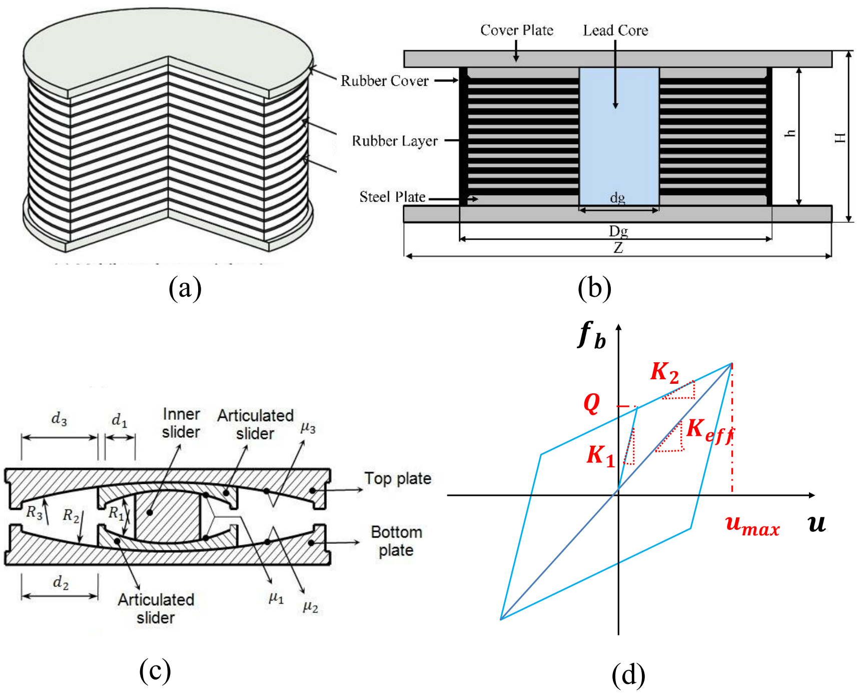

Figure 2.3. Various types of isolation bearings: (a) ERB; (b) LRB (Hu, 2014); (c) FPS; (d) bilinear model for isolation bearings.

Table 2.1. Mechanical characteristics for the three types of isolation bearings (Zhang and Huo, 2009)

Bearing type	Posityielding ratio N ($N = K_1/K_2$)	Characteristic strength Q	Postyielding stiffness K_2
ERB	5-15	From hysteresis loop	$K_2 = GA/\sum t_r$
LRB	15-30	$Q = f_y A_{lead}$	$K_2 = (1.15 - 1.20)\dfrac{GA}{\sum t_r}$
FPS	50-100	$Q = \mu W$	$K_2 = W/R$

Zhang, 2004b; Soneji and Jangid, 2007; Ozbulut and Hurlebaus, 2011b; Xie and Zhang, 2018). In the vertical direction, isolation bearings transmit the weight of the superstructure to the substructure, while they isolate the shaking effect of the superstructure in the horizontal direction. They also provide additional energy dissipations through their hysteretic mechanisms (Constantinou *et al.*, 2007). Three commonly used isolation bearings are elastomeric bearing (ERB), lead-rubber bearing (LRB), and friction pendulum systems (FPS). Their differences lie in the mechanical properties and energy dissipation mechanisms, but their hysteretic behaviours can be generally represented using a bilinear model (Naeim and Kelly, 1999). The bilinear model and the corresponding modelling parameters for the three types of isolation bearings are shown in Figure 2.3(d) and Table 2.1, respectively. Particularly, the bilinear material model is characterized by three parameters: postyielding stiffness K_2, yielding strength Q, and the postyielding ratio N (the ratio between postyielding stiffness and elastic stiffness). Different types of isolation bearings would have distinct postyielding ratios, as discussed by Zhang and Huo (2009) and summarized in Table 2.1.

Historical earthquake events (Chaudhary *et al.*, 2000; Bessason and Haflidason, 2004), experimental research (Tsopelas *et al.*, 1996) and numerical simulations (Zhang and Huo, 2009; Xie and Zhang, 2017, 2018) have proven the seismic protection effectiveness of installing isolation bearings. For instance, several studies have found that seismic damage to bridge columns (Zhang and Huo, 2009; Dion *et al.*, 2012) and span unseating (Abdel Raheem, 2009; Ghosh, Singh and Thakkar, 2011), as well as post-earthquake repair costs (Padgett, Dennemann and Ghosh, 2010; Xie and Zhang, 2017, 2018), can be significantly reduced if the bridge is equipped with base isolators. However, the effectiveness of bearing isolators is questionable if their parameters are not properly designed. This issue becomes evident for 1) flexible bridges with large natural periods (He *et al.*, 2020) and 2) bridges close to earthquake fault ruptures. First, bridges with high-elevation piers or surrounded by soft soils may have a natural period larger than the predominant period of seismic waves, in which case the period elongatioan effect of bearing isolators is negligible (Dezi *et al.*, 2012; Agrawal and Amjadian, 2022). Second, the bearing isolator works ineffectively when the bridge is subjected to the long pulse component of near-field earthquake events – the presence of isolation bearings sometimes would make the bridge system more flexible and vulnerable (He and Agrawal, 2008; Losanno, Hadad and Serino, 2017). Recent studies have also revealed possible bearing failure modes – the excessive deformation demand would cause shear failure to bearings (Mangalathu, 2017).

Extensive studies indicated potential challenges that may hinder the wide application of isolation bearings. First, the stiffness of LRB and ERB increases as temperature drops, which could induce the overloading of pier columns in cold seasons (Sato *et al.*, 1994), and they become softer if environment temperature increases or cyclic deformation generates heat. Second, isolation bearings are susceptible to loading history. Experiments and field inspections have demonstrated the reducing bulk modulus and increasing effective damping of elastomers under cyclic loading, known as Mullins' effect (Mullins, 1969) or scragging effect (Clark, 1996). Finally, the mechanical properties of aged isolation bearings could change, due to the continued vulcanization and degradation of elastomer (Constantinou *et al.*, 2007). Raw rubber gains strength and elasticity by vulcanization, and the effective shear modulus of elastomers keeps increasing with time. Degradation of rubber happens if exposed to oxygen and ozone, and this can be prevented by adding waxes and anti-oxidants to the rubber matrix.

2.2.2 Damper devices

Various damper devices with different mechanical properties have been developed during the past three decades. These devices include fluid viscous damper (FVD), friction damper, metallic damper, shape memory alloy damper (SMA) (Song, Ma and Li, 2006), and tuned mass damper (TMD), etc.

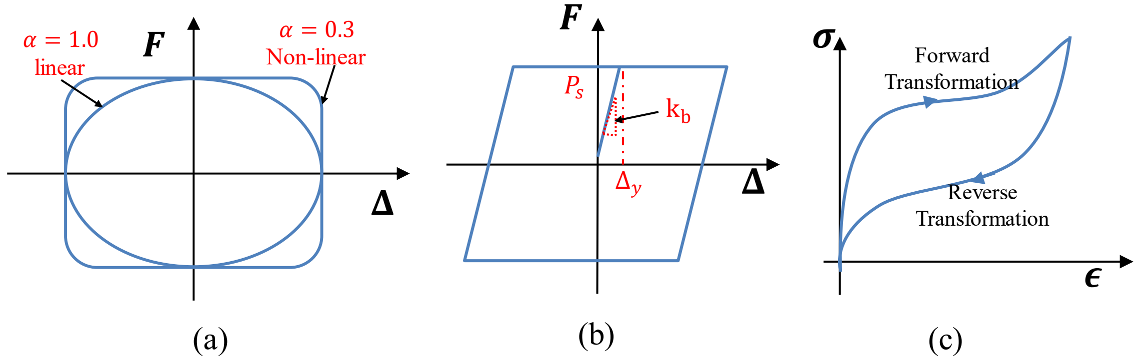

Figure 2.4. Material models for dampers: (a) FVD; (b) Friction/metallic damper; (c) SMA

FVD resists the vibration of structures by generating a force that is proportional to the relative velocity between the two ends of the damper, as shown in Eq. (2.2) (Pekcan, Mander and Chen, 1999; Xie and Zhang, 2017, 2018; De Domenico, Ricciardi and Takewaki, 2019):

$$F_d(t) = C_\alpha \cdot \mathrm{sgn}[v(t)] \cdot |v(t)|^\alpha \tag{2.2}$$

where $\mathrm{sgn}[v(t)]$ is the signum function to damper velocity $v(t)$, and C_α is the viscous coefficient for the damper. α is the velocity exponent, and it controls the nonlinearity of FVD. The FVD is linear when $\alpha = 1$, and the damper force F_d is linearly proportional to damper velocity v. Previous studies have identified that α usually takes a value from 0.3 to 1.0 toward effective seismic protection (Lee and Taylor, 2001; Narkhede and Sinha, 2014; Xie and Zhang, 2017, 2018; Berquist and DePasquale, 2020). Figure 2.4 (a) compares the force-displacement curves for linear FVD and nonlinear FVD. Although the nonlinear damper has a better energy dissipation ability, linear damping is preferred in seismic applications. The reason is that higher modes of structure are less likely to be activated by linear damping, as it has little correlation with structural forces (Lee and Taylor, 2001). In bridge engineering, numerous experimental and numerical studies have been conducted to validate the effectiveness of installing FVDs (Madhekar and Jangid, 2009; Dion *et al.*, 2011; Zhu *et al.*, 2016; Xie and Zhang, 2017, 2018).

Friction and metallic dampers exhibit similar hysteretic behaviours, as shown in Figure 2.4 (b). The material model for these two types of dampers can be characterized using three parameters: elastic stiffness (k_b), friction/yielding strength (P_s), and postyielidng stiffness (k_2). When seismic force in the damper exceeds the friction/yielding strength P_s, friction and metallic dampers start to dissipate energy through yielding and friction mechanisms, respectively. However, neither metallic nor friction devices will dissipate energy if the earthquake intensity is low, and they will provide additional elastic stiffness to the system (Moreschi and Singh, 2003). Metallic and friction dampers gain popularity in structural engineering because of their 1) stable hysteretic behaviour and energy dissipation capacity; 2) reliable performance under different temperatures; 3) simplicity in manufacturing; and 4) competitive cost-effectiveness (Westenenk *et al.*, 2019a; Javanmardi *et al.*, 2020a).

It is worth mentioning that different metal materials constitute distinct properties of metallic dampers. For example, lead dampers require no repair or replacement after earthquakes because of the recrystallization behaviour, although they are heavier and costlier than steel dampers (Javanmardi *et al.*, 2020b). The most significant disadvantage of metallic and friction dampers is the lack of self-centering capability, leaving the base structure with residual deformations after earthquake events (Westenenk *et al.*, 2019b). Applications of metallic and friction dampers can be found in frame structures (Moreschi and Singh, 2003; Kiris and Boduroglu, 2013; Ebadi Jamkhaneh, Ebrahimi and Shokri Amiri, 2019; Taiyari, Mazzolani and Bagheri, 2019), highway bridges (Xiang, Alam and Li, 2019; Xiang and Li, 2020), and cable-stayed bridges (Zhou, Wang and Ye, 2019; Wen *et al.*, 2021a).

SMA damper employs superelastic shape memory alloy material to dissipate seismic energy, and its flag-shaped hysteretic curve is shown in Figure 2.4(c). SMA damper is able to restore to the undeformed shape after experiencing large strains, with negligible residual deformation and perfect self-centering property. This unique characteristic makes SMA attractive to vibration control, and many previous studies have investigated its application in earthquake engineering (Dolce, Cardone and Marnetto, 2000; DesRoches and Delemont, 2002; Desroches and Smith, 2004; Song, Ma and Li, 2006; Gur, Xie and DesRoches, 2019). Li et al. (2004) simulated the vibration of stay cable-SMA damper combination and found that the SMA damper can suppress the vibration amplitude. Sharabash et al. (2009) utilized SMA dampers to reduce the force demand in the tower for cable-stayed bridges. Besides, these studies also pointed out that the design parameters of SMA dampers would significantly influence the effectiveness of seismic risk mitigation. Gur et al. (2019) compared the performance of SMA damper with steel yielding damper, and concluded that SMA damper outperforms yielding damper in reducing floor accelerations and inter-story drifts. SMA devices have also shown promise in the seismic retrofit of existing bridges, as verified through both numerical studies (DesRoches and Delemont, 2002; Andrawes and DesRoches, 2007) and experimental tests (Johnson *et al.*, 2008; Padgett, DesRoches and Ehlinger, 2009).

2.3 Design and optimization of seismic protective devices

Although seismic protective devices show promise in mitigating the seismic risk of civil engineering structures, their efficiency is contingent on the proper design of parameters and configurations (Constantinou *et al.*, 2007). A counterexample is the failure of the Bolu Viaduct bridge during the 1999 Ducze earthquake – the bearing's displacement capacity was exceeded substantially (Roussis *et al.*, 2003). To this end, standard seismic codes suggested systematic design methods for seismic protective devices. Taking isolation bearing as an example, the European code (2005) and American Association of State Highway and Transportation Officials

(AASHTO) (2010) give similar design methods, including 1) simplified method; 2) single-mode spectral method; 3) multimode spectral method, and 4) time-history method. The first three methods represent the bridge and nonlinear isolators by an elastic model with equivalent dynamic properties (e.g., period and damping ratio), and the design response spectrum for the construction site is used to estimate the seismic demand of key components iteratively. The design for isolation bearings can be determined once the iteration is finished and the seismic performance objective is achieved. The time history analysis method is used when the bridge exhibits irregularity (Amjadian and Agrawal, 2016) or large ductility demand (AASHTO, 2010). The method is regarded as the most accurate, although it is more time-consuming. The time history analysis method usually simulates a 3D bridge model and isolators with nonlinear material and elements, and a bilinear model (Figure 2.3(d)) can be used to simulate the hysteretic behaviour of isolators (Eurocode 8, 2005; AASHTO, 2010).

Seismic protective devices designed by standard codes don’t guarantee optimal economic performance of the system, and the associated different sources of uncertainties and reliabilities are not explicitly quantified. To this end, numerous optimization-based design methods for seismic protective devices have been proposed in the last three decades. In general, design methodologies for seismic devices can be classified to be deterministic (Wang, Chung and Liao, 1998; Makris and Zhang, 2004a; Jangid, 2005; Soneji and Jangid, 2007; Ozbulut and Hurlebaus, 2011a) and probabilistic (Karim and Yamazaki, 2007; Padgett and DesRoches, 2008; Agrawal et al., 2012; Siqueira et al., 2014; Olmos Navarrete et al., 2016). The deterministic method simulates the structure’s nonlinear time history responses under a handful of ground motions to determine its performance state. This method is conditioned on pre-defined seismic hazard levels (e.g., earthquake with a return period of 2475 years), and it fails to consider the uncertainties in earthquake hazards. Conversely, the probabilistic approach aims to design the seismic protective devices against several performance objectives by incorporating and propagating various sources of uncertainties (Mackie and Stojadinović, 2007). Therefore, recent efforts in the earthquake engineering community have focused largely on moving away from deterministic methods to performance-based methods for selecting protective devices for highway bridges.

In the last two decades, the PEER's PBEE framework has been widely used in the design of new structures (Goulet *et al.*, 2006; Mitrani-Reiser *et al.*, 2006; Mitseas, Kougioumtzoglou and Beer, 2016; Perrone and Filiatrault, 2017; Mosalam *et al.*, 2018) and assessment of existing structures (Mitrani-Reiser, 2007; Mackie, Wong and Stojadinović, 2009; Tubaldi, Barbato and Dall'Asta, 2014; Cardone and Perrone, 2017). The fragility curve is the key component in the PBEE framework. A seismic fragility curve can be established through expert opinions, empirical methods, and analytical methods. The analytical fragility curve is generally more reliable but computationally expensive, as a large number of nonlinear time history analyses are required to capture the uncertainty in seismic hazards (Mangalathu, 2017). In this regard, the PBEE-based optimal design of protective devices for highway bridges is a cumbersome and iterative process unless a more efficient and practical method is proposed. Very few studies have attempted to leverage the PBEE framework in the optimal design of seismic protective devices. Zhang and Huo (2009) have conducted an extensive sensitivity analysis to link a composite damage index to the design parameters of isolation bearings. Their work has been extended recently to incorporate the bridge seismic repair cost ratio (RCR) (Xie and Zhang, 2017, 2018) into a genetic optimization framework to identify the optimal design parameters for both the isolation bearings and viscous dampers. Wen et al. (2021) applied a similar framework to design viscous dampers for a cable-stayed bridge. Although these studies have made promising attempts, some limitations still exist that warrant further research. First, only the bridge column and bearing are considered the vulnerable components, which contradicts the fact that the seismic damage to other bridge components, such as abutment wall (Zheng *et al.*, 2021), pile foundation (Xie *et al.*, 2021), shear key, span unseating, and joint seal (Mangalathu, 2017), would also inflict substantial seismic losses. Second, the proposed performance objective (i.e., the damage index in Zhang and Huo (2009) and the RCR in Xie and Zhang (2017, 2018)) are still conditional on the intensity measure (*IM*) of ground motions, instead of a system-level risk index. As a result, the optimal design parameters can only be identified at discrete *IM* levels. Besides, significant computational efforts have to be spent to deal with the inherent challenge that a new design of seismic protective devices would alter the dynamic characteristics of the bridge and thereby change the corresponding seismic fragility curves.

Chapter 3 – Risk-based Optimization Framework for Seismic Protective Devices

The PEER recommended PBEE framework in Eq. (2.1) is applicable for a single specified structure. For individual structures with deterministic design/modeling parameters, the primary source of uncertainty comes from earthquake hazard, where the ground motion *IM* serves as the point of contact between seismic hazard and seismic demand represented by *EDP*s. In this case, seismic fragility models estimate the probability of limit state exceedance in terms of a single variable, the earthquake *IM* (Cornell *et al.*, 2002).

The PEER formulation also bears the flexibility to be expanded towards seismic risk assessment of regional structures, where work has considered analysis of archetype structures or groups of representative structures to derive *IM*-based class fragilities. To this end, recent advances supporting seismic risk assessment of regional portfolios of structures consider demand models with multiple predictors, including not only earthquake *IM* but other influential structural parameters. As such, the resultant fragility models are parameterized and can be tailored to any specific structures once their design/modeling parameters are made available [e.g., Dukes, 2013; Ghosh, Padgett and Dueñas-Osorio, 2013].

Inspired by the recent efforts of developing parameterized seismic fragility models for regional structures, this study adopts and adapts the associated analysis workflow into the optimal design of seismic protective devices for a multi-component structure system. As shown in Fig. 3.1, other than the existing analysis procedure recommended by the PEER center, additional analysis modules include (1) the design of experiment (Park, 2007) for a wide collection of seismic

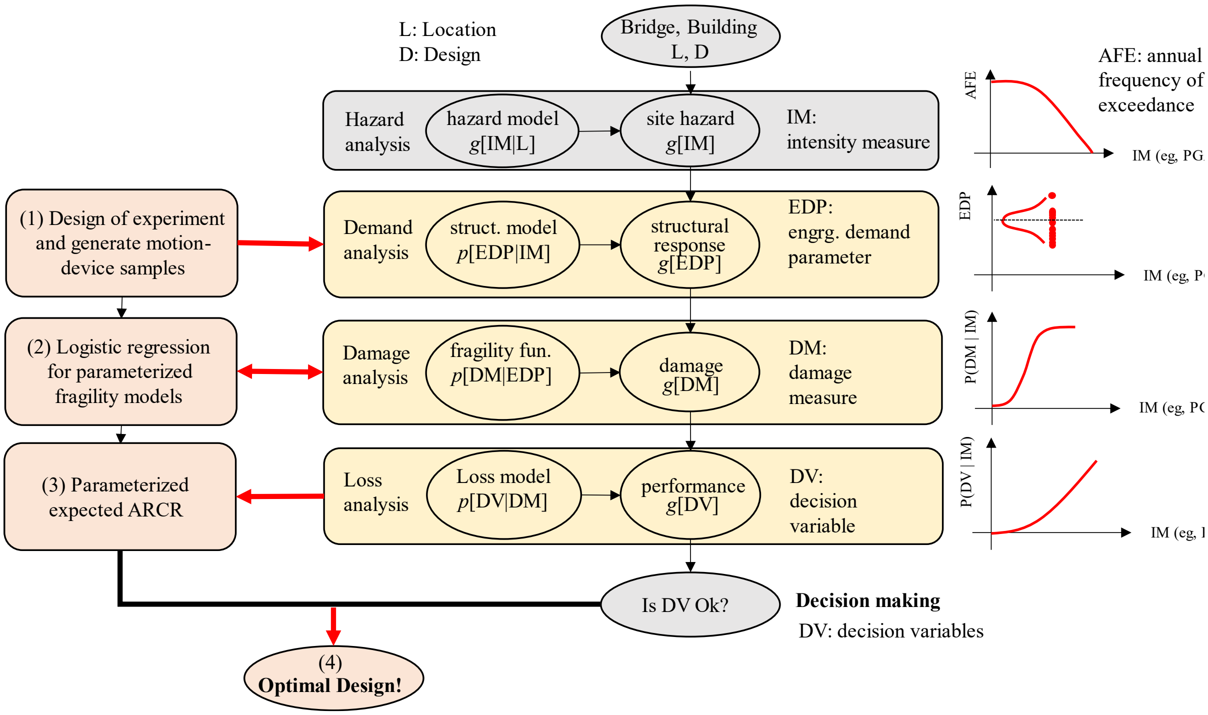

Figure 3.1. Risk-based Optimization Flowchart of Seismic Protective Devices

protective devices and generating motion-device samples for seismic demand analysis; (2) comparing the demand versus capacity for each numerical sample and using the logistic regression to develop the parameterized fragility models; (3) combining the fragility results with hazard models and loss estimates to develop parameterized, expected annual repair cost ratio (ARCR); and (4) pinpointing the optimal design by directly visualizing the global minimum of the ARCR surface.

The proposed flowchart features two advantages compared with previous attempts that involve performance-based approaches to design bearings and dampers [e.g., Zhang and Huo, 2009; Xie and Zhang, 2017, 2018]. First, one set of computations is sufficient to parameterize the fragility and risk models as functions of the design parameters of devices. Namely, all possible design scenarios have been captured at once, including the change of dynamic characteristics of the system (e.g., damping ratio, stiffness) due to the installation of different devices. By contrast, Zhang and Huo (Zhang and Huo, 2009) used permutations to include all design scenarios and computed the fragility curve for each combination of design parameters. Moreover, both (Xie and Zhang, 2017) and (Xie and Zhang, 2018) relied on genetic algorithms to identify the optimal design under each ground motion. Hundreds or even thousands sets of computations are needed in these studies. The development of parameterized fragility models avoids a highly iterative and tedious process since fragility models can be automatically updated against new design scenarios. Second, this study directly links the design parameters of devices to the *DV* (i.e., ARCR) of the system, which integrates all the intermediate variables such as *IM*, *EDP*, and *DM*, as well as the damage potential of all constitutive components. Note that this direct linkage explicitly quantifies and eliminates the dependency between the DV and IM, which has not been fully achieved in the existing literature [e.g., Zhang and Huo, 2009; Xie and Zhang, 2017, 2018]. As such, the proposed workflow moves forward from a performance-based approach into a complete system-level, risk-based methodology. Moreover, the explicit functional relationship between ARCR and design parameters of devices enables a convenient identification of the optimal bearing and damper designs by directly visualizing the global minimum of the convex ARCR surface. Given the overall methodology, individual analysis modules and crucial considerations are introduced separately in the following sections.

3.1 Seismic hazard model

As the first step, the seismic hazard model predicts the annual probability of exceeding some intensity levels of earthquake events. Probabilistic seismic hazard analysis is a widely adopted approach to develop seismic hazard models by taking into account all possible sources of uncertainties, such as location, fault type, and epicenter distance (Baker, 2015; Gerstenberger *et al.*, 2020). One example of seismic hazard models is developed by the United States Geological

Survey (2020, last access, 2021-07-24), where the annual exceedance probabilities of earthquakes are provided concerning different *IMs*. For ease of implementation, the hazard data at discrete *IMs* can be commonly regressed as a continuous hazard curve, including the exponential model (Eq. (2.1)) or hyperbolic model (Eq. (3.2)).

$$\lambda(IM) = a\ (IM)^b \tag{3.1}$$

$$\lambda(IM) = \alpha \exp\left[\beta\ \left(\ln\left(\frac{IM}{\gamma}\right)\right)^{-1}\right] \tag{3.2}$$

where a, b, α, β, γ are regression constants determined by fitting over the hazard data. Eq. (3.1) assumes that λ and IM are in a linear relationship in the log-log space, while Eq. (3.2) shows a hyperbolic relationship in the log-log space. Although the linear relationship is simpler in computation, the hazard data does not always precisely follow this simple trend (Bradley *et al.*, 2007). The hyperbolic relationship in Eq. (3.2) is used in this study to consider both linear and nonlinear logarithmic hazard probabilities (Bradley *et al.*, 2007; Kameshwar and Padgett, 2014). Using this hazard model, selections of *IM* and ground motions will be discussed in the next section in the context of a bridge case study.

3.2 Seismic response modeling of a multi-component bridge system

The fragility curve in this study is derived through an analytical approach, which thereby requires the numerical modeling and damage analysis of the concerning structure. Taking highway bridge as an example, significant progress has been made to understand the seismic damage of different bridge components. Previous seismic design and evaluation efforts focus on detailing the bridge column, which has been considered the most vulnerable component in a bridge system (Xiao *et al.*, 2011; Gulerce *et al.*, 2012; Lee *et al.*, 2021). The vulnerabilities of the remaining bridge components and their design details might be controlled by different hazards other than earthquakes (Petrini *et al.*, 2020). However, recent studies have also examined the seismic vulnerability of other components, including abutment backwall (Zheng *et al.*, 2021), shear key, bearing (Xie and Zhang, 2018), joint seal, and foundation (Xie *et al.*, 2021), etc. Although the damage of these structural components is generally less likely to cause the complete collapse of the bridge, their inclusion in the seismic risk assessment is of significant importance to bear accurate risk quantifications at the bridge system level (Akkari et al., 2015).

In addition, the design and optimization of seismic protective devices also need to consider multiple bridge components. This is because the installation of isolators and dampers will redistribute the damage potential across these different components. For example, a base isolator with larger stiffness can effectively reduce the bearing damage and the potential of span unseating. However, this larger bearing stiffness permits enlarged inertia force to be transmitted to substructures, which would increase the damage probabilities of the column, abutment, and foundation at the same time. To this end, designing seismic protective devices should expect conflicting responses and damage probabilities among column, bearing, span unseating, foundation, and abutment components. Therefore, a high-fidelity numerical model is needed to capture the seismic damage and loss of all constitutive elements in a bridge system. Detailed considerations of such a numerical model will be discussed in Chapter 4.

3.3 Design of experiment and parameterized fragility models

The parameterized fragility models developed herein estimate the damage/failure probabilities of bridge components conditioned on earthquake *IM* and design parameters of bearings and dampers. To construct a robust fragility model, sufficient bridge response data when subjected to different design parameters and earthquake ground motions are needed to account for all possible sources of uncertainties. In this regard, a design of experiment (Kameshwar and Padgett, 2014) is carried out for a given bridge structure to statistically sample a large set of stochastic realizations for bearing/damper designs and ground motion inputs. The most frequently used sampling schemes include Latin Hypercube Sampling (LHS) (Mckay, Beckman and Conover, 2000), Monte Carlo sampling (Niederreiter, 1992), and orthogonal array sampling (Nordhausen, 2009). Because this study aims to search the optimal bearing/damper design parameters from the high dimensional design space, these design parameters are assumed to follow independent uniform distributions sampled by the LHS method. At the same time, a large suite of ground motions is selected to be consistent with the seismic hazard at the bridge site.

Subsequently, nonlinear time history analysis (NLTHA) is performed against every ground motion-device pair for the bridge. Seismic demands of different bridge components are recorded from the NLTHAs through *EDPs* and are compared with their associated capacity limit states of reaching different damage states. The seismic capacities of bridge components can be determined based on expert's opinions, experimental testing, field measurement, and computational simulation (Nielson, 2005). By comparing the seismic demand with the capacity, the binary survival-failure vector indicating the failure ratio of each bridge component against each damage state can be computed. As such, parameterized seismic fragility models can be developed using a multi-input, multi-output dataset with the design parameters of bearings/dampers and earthquake *IMs* as the predictors, and the survival-failure values of each bridge component reaching different damage states as the labels. This study adopts logistic regression to develop the fragility models because of its consistent statistical inference – a logistic regression curve also predicts the probability of reaching a failure (Xie *et al.*, 2020). To yield more accurate regression results, a second-order polynomial response surface model (PRSM) is incorporated into the logistic regression (Cundy *et al.*, 2003; Seo and Linzell, 2012; Ghosh, Padgett and Dueñas-Osorio, 2013), as shown in Eqs. (3.3) and (3.4):

$$P[Fail|\, X, IM] = \frac{e^{g(X,IM)}}{1 + e^{g(X,IM)}} \tag{3.3}$$

$$g(X, IM) = \beta_0 + \sum_{i=1}^{k} \beta_i x_i + \sum_{i=1}^{k} \sum_{j=1, j<i}^{k} \beta_{ij} x_j x_i \tag{3.4}$$

where X represents design parameters of seismic protective devices, $P[Fail|X, IM]$ denotes the parameterized damage probability (i.e., fragility model) conditioned on the design parameters *X* and earthquake *IM*, *k* is the total number of cases for NLTHAs, and $\beta_0, \dots, \beta_{ij}$ are unknown coefficients that are determined by using the maximum likelihood estimation approach. To this end, Eq. (3.4) defines the parameterized seismic fragility model for each bridge component that can be further utilized for system-level risk assessment.

3.4 Parameterized, expected annual repair cost ratio (ARCR)

Seismic risk assessment is further conducted to eliminate the dependence of earthquake *IM* and combine the damage potential of different bridge components. A bridge system-level seismic loss analysis is considered in this study, where the expected annual repair cost ratio (ARCR) is computed by coupling the seismic hazard model, component-level fragility model, and the associated loss quantifications. In particular, the expected ARCR is derived in two steps. First, seismic-induced loss of the bridge is quantified through the repair cost ratio (RCR) that combines the contribution of each bridge component (Xie and Zhang, 2017, 2018). The closed-form formula of RCR is provided in Eq. (3.5), where *l* and *m* are the subscripts indicating damage states and bridge components, respectively, *L* is the total number of damage states, $d_{l,m}$ is the damage ratio describing the percentage damaged for component *m* in state *l*, and c_m is the replacement cost of component m, $p_{l,m}$ is the probability of the m_{th} component staying in damage state l, which can be computed through Eq. (3.6).

$$RCR(X, IM) = \frac{\sum_{l=1} \sum_{m=1} p_{l,m}(X, IM) d_{l,m} c_m}{\sum_m c_m} \tag{3.5}$$

$$p_{l,m}(X, IM) = \begin{cases} P_{l,m}(X, IM) - P_{l+1,m}(X, IM), & \text{for } 1 \leq l \leq L-1 \\ P_{L,m}(X, IM) \qquad\qquad\qquad , & \text{for } l = L \end{cases} \tag{3.6}$$

In essence, The *IM*-based RCR formula quantifies the seismic vulnerability of the bridge in terms of economic losses (FEMA, 2021). It combines the component-level fragility models (i.e., $P_{l,m}(X, IM)$ in Eq. (3.6)) with the exposure information (i.e., replacement cost c_m and damage ratio $d_{l,m}$ in Eq. (3.5)) of the bridge. The fragility models $P_{l,m}(X, IM)$ are provided in Eq. (3.3) as functions of earthquake *IM* and design parameters *X*, while the exposure information can be determined according to the bridge configuration, construction material, seismic design levels, etc. (Ghosh *et al.*, 2014; Mangalathu, 2017).

To eliminate the dependence on earthquake *IM*, the expected ARCR is further computed through Eq. (3.7) that convolves the seismic RCR of the bridge with the mentioned seismic hazard model (i.e., Eq. (3.2)). It is worth mentioning that the ARCR formula has been deemed a reliable estimate of the seismic risk in a short time period (Kiureghian, 2005). In the current work, the ARCR also has its unique feature as a parameterized function that directly links *X*, the design parameters of seismic protective devices, to the expected annual repair cost of the bridge. As such, the optimal design scenario can be intuitively identified by visually pinpointing the design parameters that yield the minimum ARCR.

$$ARCR(X) = \int_{IM} RCR(X, IM) \left| \frac{d\lambda}{d(IM)} \right| d(IM) \tag{3.7}$$

Chapter 4 - Case Study: Retrofitting an Early-Designed Benchmark Bridge with Optimally Designed Seismic Protective Devices

4.1 The benchmark bridge and its numerical modeling

As one of the prevalent types of bridges in California, the multi-span continuous concrete box-girder bridges were seismically vulnerable during previous earthquake events, such as the 1994 Northridge Earthquake and the 1989 Loma Prieta Earthquake (Mitchell, Tinawi and Sexsmith, 1991; Mitchell *et al.*, 1995). In addition, recent research has also underscored the temporal dependence of bridge performance when subjected to earthquake loading. Namely, the bridges in California that are designed before 1971 (Era 1) are seismically most vulnerable due to the lack of seismic detailing and ductility (Ramanathan, 2012). As such, this study selects the two-span, single-column continuous concrete box-girder bridge designed in Era 1 with seat-type abutments as the benchmark case for seismic retrofitting. A comprehensive review of the bridge inventory indicates significant variations in geometric parameters, material properties, and design details for the benchmark bridge class, where statistical distributions of the relevant modeling parameters have been summarized in previous studies (Ramanathan, 2012; Mangalathu, 2017). To be representative, the median values from each distribution (i.e., those tabulated in Table 4.1) are used to benchmark the case-study bridge.

The modeling parameters shown in Table 4.1 provide data inputs to build a high-fidelity numerical model of the benchmark bridge for seismic response/demand modeling. As shown in Fig. 4.1, the software platform of OpenSees (McKenna, 2011) is utilized to develop a detailed three-dimensional finite element model that features the following considerations. First, the bridge deck is simulated using elastic beam elements with mass lumped along the centerline. The

Table 4.1. Parameters considered in the bridge model

Items/Components	Parameters	Value
Geometry	Span length, $L_m(m)$	31.85
	Deck width, $D_w(m)$	10.97
	Column height, $H_c(m)$	7.00
Column	Concrete compressive strength, $f_c(MPa)$	27.90
	Rebar yielding strength, $f_y(MPa)$	404.60
	Longitudinal reinforcement ratio, ρ_t	2.23%
	Transverse renforcement ratio, ρ_t	0.90%
Pile group	Translational stiffness, $K_{ft}(kN/mm)$	270.7
	Transverse rotational stiffness, $K_{fr}(GN \cdot m/rad)$	3.55
	Transverse/longitudinal rotational stiffness ratio, k_r	1.50
Abutment on piles	Abutment backwall height, $H_a(m)$	2.18
	Pile stiffness, $K_p(kN/mm)$	0.15
	Backfill capacity, P_c (*kN*)	2105.02
Gap	Longitudinal gap (pounding), $\Delta_l(mm)$	23.04
	Transverse gap (shear key), $\Delta_t(mm)$	12.85
Shear key	Acceleration for shear key capacity, $a_{sk}(g)$	1.00
Mass	Mass factor, m_f	1.05
Damping	Damping ratio, ξ	0.05

connections between the bridge deck and end abutments are preserved through rigid transverse beams. The columns are simulated using displacement-based beam-column elements with discretized fiber-defined sections to specify distinct nonlinear material properties at different locations across the cross-section. It is worth mentioning that the confinement effect of stirrups partitions the cross-section into core concrete and cover concrete, where the core concrete features larger strength and ductility. In particular, the Concrete02 material is used to model the concrete, and material properties for the confined concrete are computed using the Mander's model (Filippou, Popov and Bertero, 1983). The Steel02 material is utilized to simulate the steel reinforcement in the column section (Filippou, Popov and Bertero, 1983). The Zero-Length-Section element is added at the bottom of the column to model the strain penetration effect

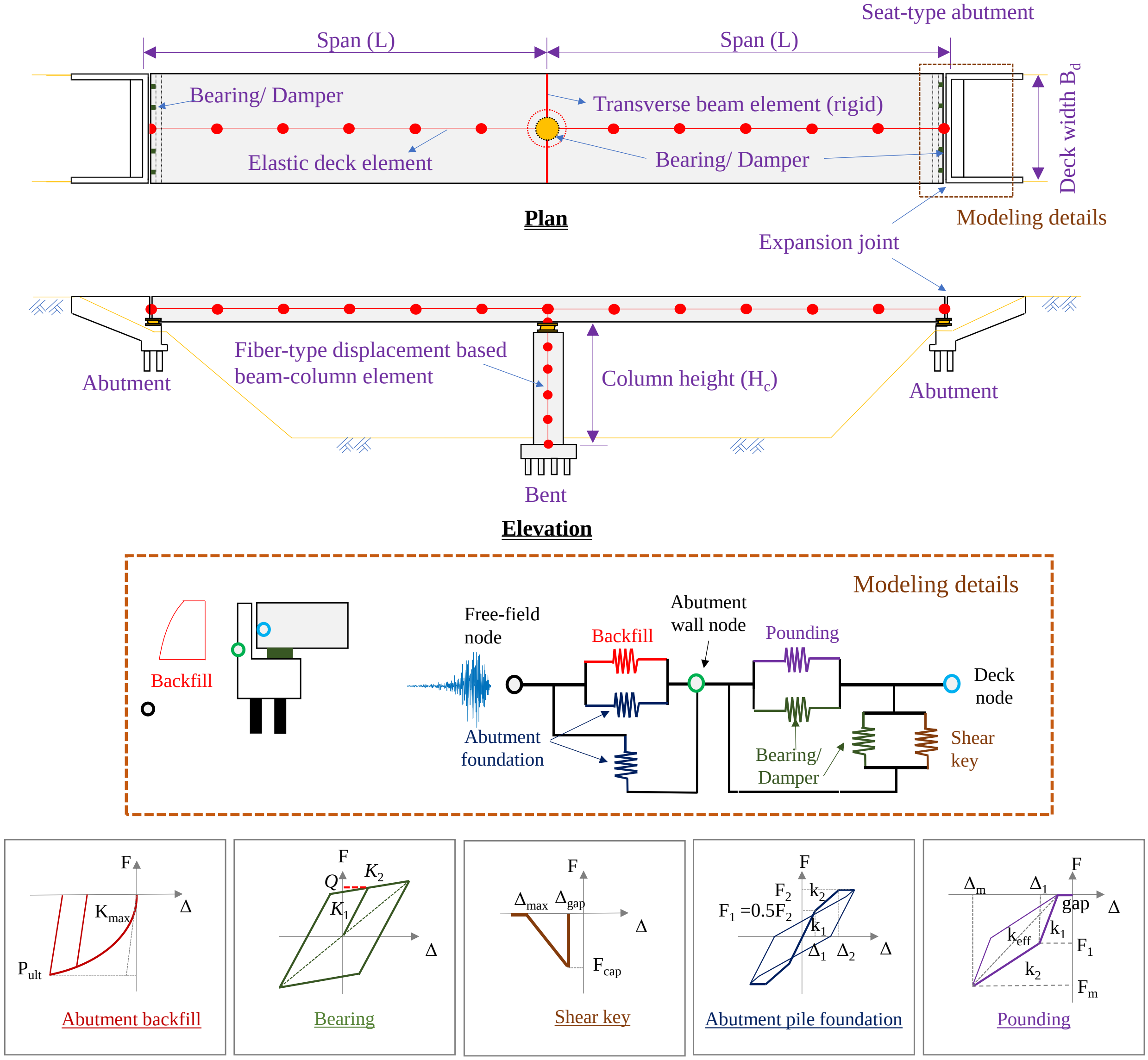

Figure 4.1. Numerical modeling of various bridge components for the case-study bridge

(Moridani and Zarfam, 2013). Elastic translational and rotational springs are used to model the column foundation, while a spring system is established to simulate the dynamic interplay among various abutment components, including abutment backfill, bearing, shear key, and abutment pile foundation. To be specific, the trilinear material model is used to model the abutment pile foundation. The contact element developed by Muthukumar and DesRoches (2006) is adopted to simulate the pounding effect between the deck and abutment wall. The shear keys' force-displacement response is modeled using a trilinear curve based on the Caltrans-UCSD field experiments (Silva, Megally and Seible, 2009), while a hyperbolic material is considered to simulate the seismic resistance of abutment backfills. Fig. 4.1 also illustrates the connection details of these abutment components and their respective constitutive curves. It is noted that the numerical models of the isolation bearings and viscous dampers will be discussed in the next section.

4.2 Design consideration of seismic protective devices

Seismic retrofit of the benchmark bridge is conducted through two different design scenarios. The first scenario considers complete isolation of the bridge by installing isolation bearings at both column top and end abutments, and the second scenario further couples the bearings with fluid viscous dampers (Fig. 4.1). It is noted that multiple bearings and dampers can be installed in parallel at each end abutment, while such a location variation is not considered herein for simplicity purposes. Instead, the seismic protective devices at each end abutment adding together are assumed to possess identical mechanical properties (i.e., stiffness and strength) as those installed at the top of the column. Moreover, each design scenario considers three cases that respectively install three different types of isolation bearings, including the elastomeric bearing (ERB), lead-rubber bearing (LRB), and friction pendulum systems (FPS). Although these three types of isolation bearings are different in configurations and materials, their seismic behaviors can be generally captured through a bilinear force-displacement model (Fig.4.1) that consists of three parameters, the yielding strength Q, elastic stiffness K_1, and post-yielding stiffness K_2. Previous experimental studies indicated that each bearing type features a distinct value of the post-yielding ratio $N = K_1/K_2$ (Zhang and Huo, 2009), where the associated typical ranges of N are listed in Table 4.2. To this end, the stiffness parameters of isolation bearings, i.e., K_1 and K_2, are somewhat dependent with each other. Besides, previous studies have concluded that the elastic stiffness K_1 bears negligible influence on the seismic performance of bridge structures when subjected to strong earthquakes (Makris and Zhang, 2004a; Zhang and Huo, 2009; Xie, Huo and Zhang, 2017). Therefore, the post-yielding stiffness K_2 and yielding strength Q are regarded as the design parameters for isolation bearings, while the elastic stiffness K_1 is determined by stochastically sampling the post-yielding ratio N for each bearing type.

The design of experiment for K_2 and Q is considered compatible with the seismic performance of the bridge, as the installation of bearings will shift the dynamic periods of the system and redistribute the damage potential of several bridge components. In this study, the column stiffness and strength are used to normalize K_2 and Q respectively, such that their choices of values can be constrained into reasonable design ranges. As shown in Fig. 4.2, a pushover analysis is conducted on the bridge column using nonlinear beam-column elements with fiber cross-sections. The force-displacement pushover curve of the column can be further simplified as an elastic perfectly plastic relationship, which provides the column's elastic stiffness $K_{1,c} = 391\ MN/m$, and yielding strength $Q_c = 5806.3kN$. Therefore, the optimal design of isolation bearings is equivalent to finding the optimal stiffness ratio ($K_r = K_2/K_{1,c}$) and strength ratio ($Q_r = Q/Q_c$) that yield the minimized seismic risk of the bridge. To this end, the design of experiment considers independent uniform distributions for K_r and Q_r, where the associated distribution ranges are listed in Table 4.2.

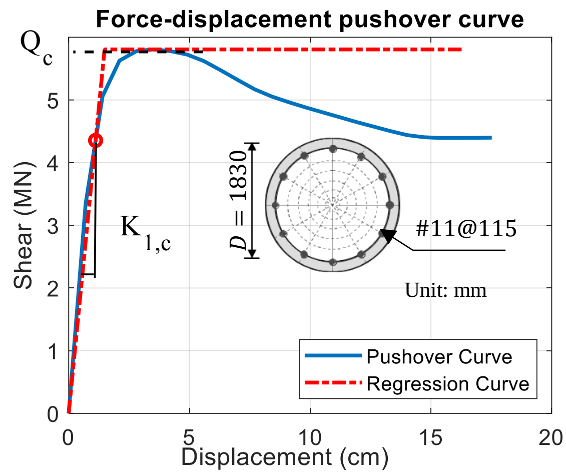

Figure 4.2. Pushover analysis of the bridge column

Table 4.2. Design parameters and their ranges considered for the seismic protective devices

Seismic protective device	Design parameters			
	$N = K_1/K_2$	$K_r = K_2/K_{1,c}$	$Q_r = Q/Q_c$	$\xi = \Sigma C_\alpha / 2m\bar{\omega}$
Bearing				
ERB	5-15			
LRB	15-30	0.01-0.06	0.1-0.6	-
FPS	50-100			
Fluid viscous damper	-	-	-	0.05-0.6

In addition to isolation bearings, the fluid viscous damper can be simulated using the constitutive law provided in Eq. (2.2). It gives the general formula for expressing the mechanical behavior of nonlinear viscous dampers, as is the case when α is smaller than one. Because nonlinear dampers can be transformed to equivalent linear dampers by matching the dissipated energy (M.D.Symans and M.C.Constantinou, 1998; Pekcan, Mander and Chen, 1999), the linear viscous damper ($\alpha = 1$) is used in this study to retrofit the bridge structure. In this case, the viscous coefficient C_α is the only parameter required to be optimized for fluid viscous dampers. The additional damping provided by all viscous dampers can be estimated using $\xi = \Sigma C_\alpha / 2m\bar{\omega}$, according to all the dampers (ΣC_α) implemented in the bridge, the mass (m) of the deck, and the natural frequency ($\bar{\omega}$) of the bridge (Xie and Zhang, 2018). Therefore, the design of experiment considers a uniform distribution of ξ that ranges from 0.1 to 0.6, which further indicates that the C_α for dampers at one location (i.e., column top or end abutment) varies from $175\ kN \cdot s/m$ to $1050\ kN \cdot s/m$.

4.3 Selections of IM, seismic hazard model, and ground motion suite

Reliable fragility outcomes depend on a proper selection of the seismic *IM*. Extensive efforts have been made previously to identify the optimal *IM* for seismic fragility models, where the selection criteria often include practicality, effectiveness, efficiency, sufficiency, etc. (Baker and Cornell, 2005; Luco and Cornell, 2007; Porter, Kennedy and Bachman, 2007; Padgett, Nielson and DesRoches, 2008). Among various *IMs*, the peak ground acceleration and spectral acceleration at a given vibrational period have been commonly considered as viable *IM* candidates, while recent studies have also shown performance improvement when using more advanced *IMs*. One particular *IM* that stands out lies in the average spectral acceleration $AvgSA(T_1)$, which can be calculated as the geometric mean of spectral accelerations at periods $c_1T_1, c_2T_1, \ldots, c_NT_1$ (where $T_1 = 0.5\ s$ is the first natural period of the benchmark bridge, and $c_1, c_2, \ldots, c_N$ are coefficient constants), as shown in Eq. (4.1).

$$AvgSA(T_1) = \left(\prod_{i=1}^{N} Sa(c_iT_i)\right)^{1/N} \tag{4.1}$$

$AvgSA(T_1)$ has shown promise to be used in building response prediction (Kohrangi *et al.*, 2017; Kohrangi, Vamvatsikos and Bazzurro, 2017) and collapse risk analysis (Eads, Miranda and Lignos, 2015). This study computes $AvgSA(T_1)$ as the geometric mean of spectral accelerations at the period interval $[0.2 \cdot T_1,\ 1.5 \cdot T_1]$ with an incremental step of $0.1 \cdot T_1$. As such, the effect of period change due to (1) the installation of new protective devices and (2) plasticity and accumulation of seismic damage can be well captured in the development of fragility models.

The benchmark bridge in this study is assumed to be physically located in the city of Los Angeles [i.e., geographic coordinates: (34.04, -118.15)] in California, United States. The associated hazard data for spectra accelerations at $T_1 = 0.5\ s$, *Sa*(0.5), can be found from the USGS website, whereas Eq. (3.2) is utilized to regress the hazard data against a continuous hazard curve. It is found that the equation with values of $\alpha = 452.07, \beta = 52.72$, and $\gamma = 49.65$ could fit the data points well. For each *Sa*(0.5) value, the associated spectra acceleration values at periods from $0.2T_1$ to $1.5T_1$ are computed using the conditional mean spectrum (CMS) curve developed by Baker (2011). Subsequently, Eq. (4.1) is used to establish a relationship between $AvgSA(T_1)$ and *Sa*(0.5), which is further utilized to develop the hazard curve for $AvgSA(T_1)$. The seismic hazard model for $AvgSA(T_1)$ is presented in Fig. 4.3, together with those represented by *Sa*(0.5) and *Sa*(1.0).

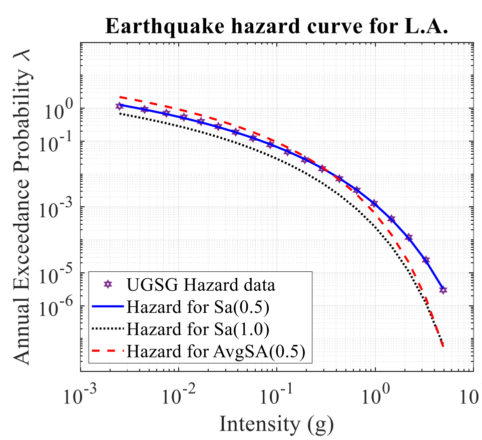

Figure 4.3. Seismic hazard models considered for the benchmark bridge

Uncertainties in earthquake loading are further captured by selecting a large number of ground motions. In this study, 615 ground motions from the NGA West 2 database (Ancheta *et al.*, 2014) are selected using the CMS developed by Baker and his co-workers (Baker, 2011; Baker and Lee, 2018). Fig. 4.4(a) shows the response spectra of the selected ground motion suite with the target CMS conditioned on $Sa(T_1)$. Moreover, the selected 615 ground motions are further scaled such that the average response spectrum of these motions bears a matching $AvgSA(T_1)$ over the periods from $0.2T_1$ to $1.5T_1$ to the target spectrum over the same period range. As a result, Fig. 4.4(b) shows the distribution of the $AvgSA(T_1)$ from the selected ground motions, where a wide range of values can be observed.

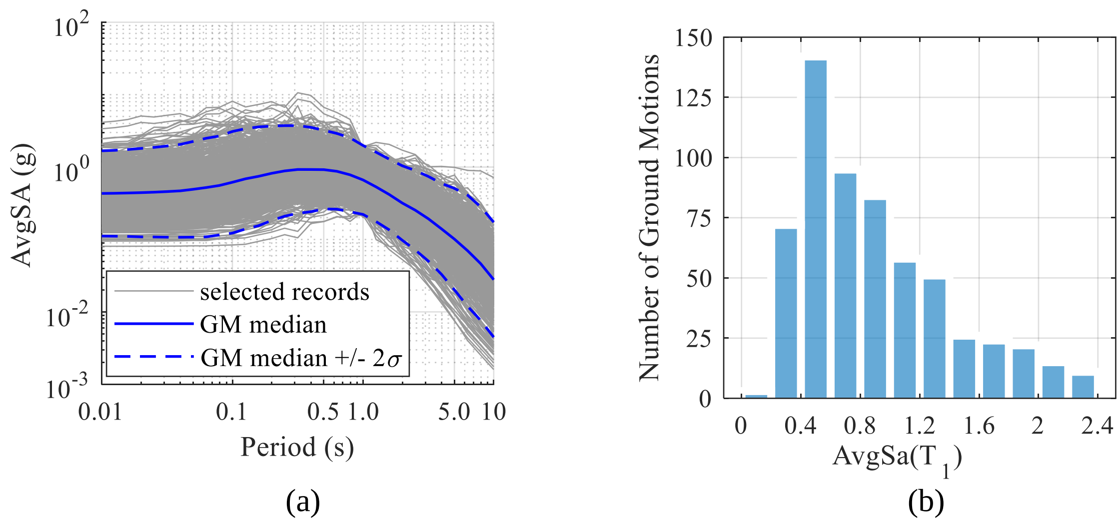

Figure 4.4. Selection of ground motions: (a) response spectra of the ground motion suite; and (b) the number distribution of AvgSA(T_1)

4.4 *EDPs* and seismic capacity models

As previously discussed, parameterized fragility models will be developed for multiple bridge components to capture their potentially conflicting damage probabilities. As shown in Table 4.3, seven bridge components are considered in the current study for seismic response monitoring through different *EDPs*. To bear a consistent risk assessment of the bridge at the system level, these seven components are classified into primary components, the failure of which would render an unstable structural system, and secondary components, which are less likely to cause a complete failure of the bridge (Mangalathu, 2017). As two primary components, pier columns and isolation bearings are considered to have four damage states (i.e., slight, moderate, extensive, and collapse damage) defined by HAZUS (FEMA, 2021), whereas the remaining secondary components are deemed to have two or three damage states (Ghosh and Padgett, 2011; Mangalathu, 2017). Other than seismic response monitoring for demand modeling, capacity limit state thresholds are defined for all bridge components reaching different damage states. As listed in Table 4.3, the lognormally distributed median and dispersion values of the limit state models are determined by synthesizing results from previous studies (Padgett, 2007; Ghosh and Padgett, 2011; Ramanathan, 2012; Mangalathu, 2017; Xie and Zhang, 2018).

Table 4.3. EDPs and capacity limit state models of different bridge components

Component	*EDP* (*unit*)	Capacity Limit State Models							
		Median				Dispersion (all EDPs)			
		S*	M*	E*	C*	S*	M*	E*	C*
Column	Drift ductility	1.0	2.0	3.0	4.0				
Unseating	Displacement (*mm*)	12.7	76.2	-	-				
Bearing	Shear strain	1.0	1.5	2.0	2.5				
Abutment	Displacement (*mm*)	18.0	108.0	218.0	-	0.25	0.25	0.47	0.47
Foundation	Rotation (*rad*)	0.002	0.005	-	-				
Shear key	Displacement (*mm*)	25.4	127.0	-	-				
Joint seal	Displacement (*mm*)	50.8	127.0	-	-				

*S for slight, M for moderate, E for extensive, and C for collapse.

4.5 Parameterized seismic fragility models

For each of the six design cases (i.e., three bearing cases and three bearing plus damper cases), 615 stochastic samples are established by randomly pairing a ground motion with randomly designed bearings/dampers. NLTHAs are carried out on each bridge-motion-device model to obtain the seismic demands, which are further compared with the stochastic samples generated from the capacity models. As such, a binary survival-failure indicator can be developed for each bridge component reaching each damage state. To this end, Eq. (3.3) is utilized to develop the associated parameterized fragility models. It is worth mentioning that the fragility models vary per bridge component, damage state, and bearing/damper design case. Due to the limited space, two sets of the models are provided herein – the fragilities of the column and bearing under the moderate damage state when the bridge is installed with the LRB, as shown in Eq. (4.2), and the fragilities of unseating and abutment reaching the slight damage state when the bridge is installed with the FPS and viscous dampers, as given in Eq. (4.3):

$$P_{col-mod}[D > C|s, q, k] = \frac{e^{-4.06+3.97q-5.10k+1.56\,q^2-0.73qk-0.69k^2+4.80s}}{1 + e^{-4.06+3.97q-5.10k+1.56\,q^2-0.73qk-0.69k^2+4.80s}} \quad (4.2a)$$

$$P_{bear-mod}[D > C|s, q, k] = \frac{e^{-9.89-3.07q-0.77k+0.22\,q^2-0.50qk+0.23k^2+5.68s}}{1 + e^{-9.89-3.07q-0.77k+0.22\,q^2-0.50qk+0.23k^2+5.68s}} \quad (4.2b)$$

$$P_{uns-slt}[D > C|s, q, k, \epsilon] = \frac{e^{16.04+2.99q+9.21k-0.76\epsilon+0.98q^2+1.03k^2-0.98\epsilon^2+0.57qk+0.24q\epsilon+1.00k\epsilon+5.82s}}{1 + e^{16.04+2.99q+9.21k-0.76\epsilon+0.98q^2+1.03k^2-0.98\epsilon^2+0.57qk+0.24q\epsilon+1.00k\epsilon+5.82s}} \quad (4.3a)$$

$$P_{abt-slt}[D > C|s, q, k, \epsilon] = \frac{e^{14.9+0.10q+3.37k+0.35\epsilon-1.22\,q^2+0.67k^2+0.35\epsilon^2-0.24qk+0.55q\epsilon-0.71k\epsilon+5.87s}}{1 + e^{14.9+0.10q+3.37k+0.35\epsilon-1.22\,q^2+0.67k^2+0.35\epsilon^2-0.24qk+0.55q\epsilon-0.71k\epsilon+5.87s}} \quad (4.3b)$$

where $q = \ln(Q_{ratio})$, $k = \ln(K_{ratio})$, $\epsilon = \ln(\xi)$, and $s = \ln(AvgSA(T_1))$, and subscripts *col* refers to column, *bear* means bearing, *uns* denotes unseating, *abt* means abutment, and *mod* and *slt* represent moderate and slight damage states, respectively.

The parameterized fragility models of each bridge component are further visualized by assigning specific values to the design parameters of seismic protective devices. Fig. 4.5 presents the component-level fragility curves of the benchmark bridge when subjected to the moderate damage state. The bridge is installed with LRBs that consider four cases of design parameters – Case 1 with $Q_r = 0.1$ and $K_r = 0.01$, Case 2 with $Q_r = 0.5$ and $K_r = 0.01$, Case 3 with $Q_r =$

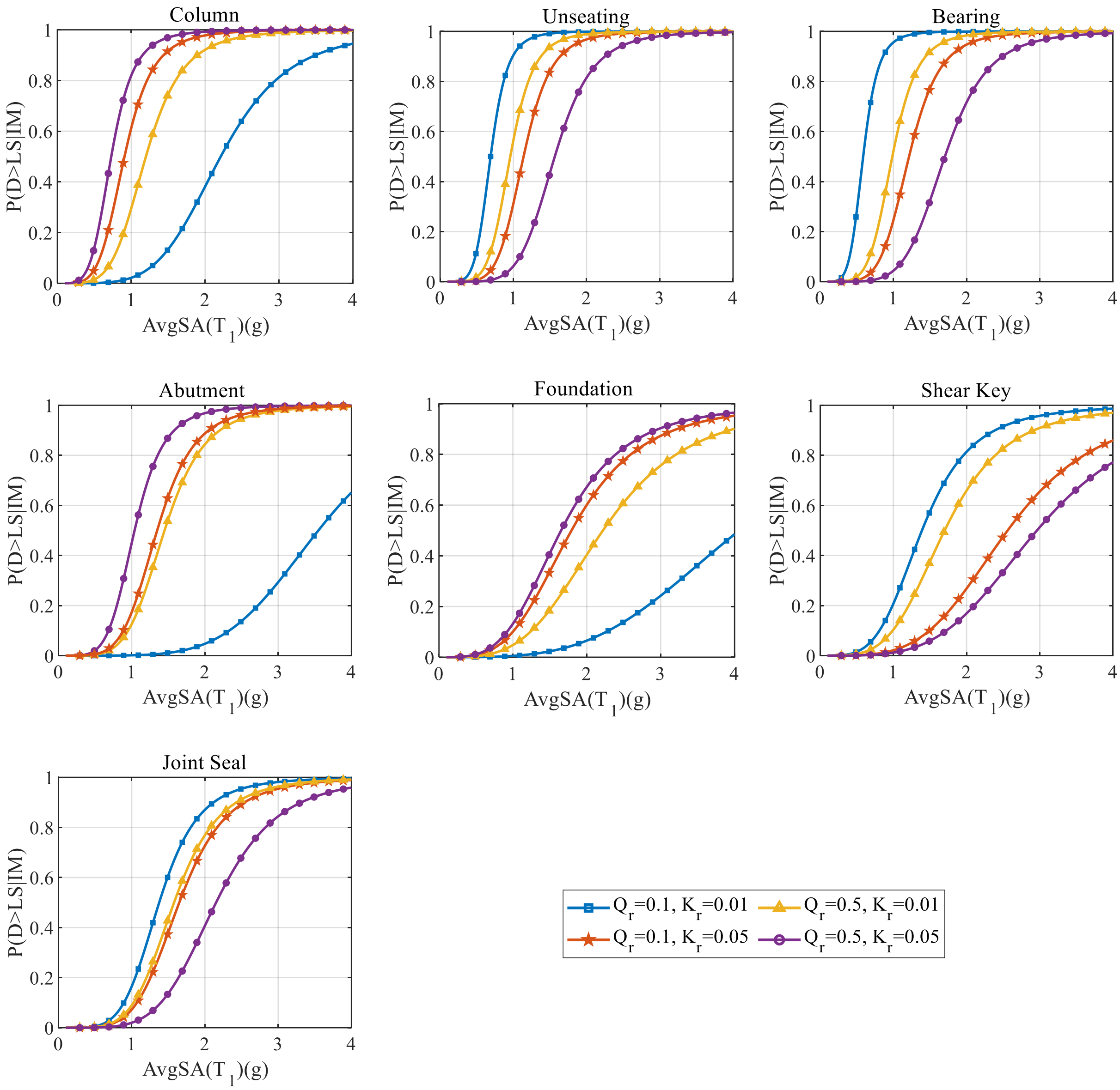

Figure 4.5. Parameterized fragility models for the LRB case under moderate damage state: (a) column; (b) unseating; (c) bearing; (d) abutment; (e) foundation; (f) shear key; and (g) joint seal

0.1 and $K_r = 0.05$, and Case 4 with $Q_r = 0.5$ and $K_r = 0.05$. Namely, both strength and stiffness values of the LRBs are increased from Case 1 to Case 4, which would cause a redistribution of the seismic fragilities across multiple bridge components. For instance, components that show increased fragilities from Case 1 to Case 4 include column, abutment, and

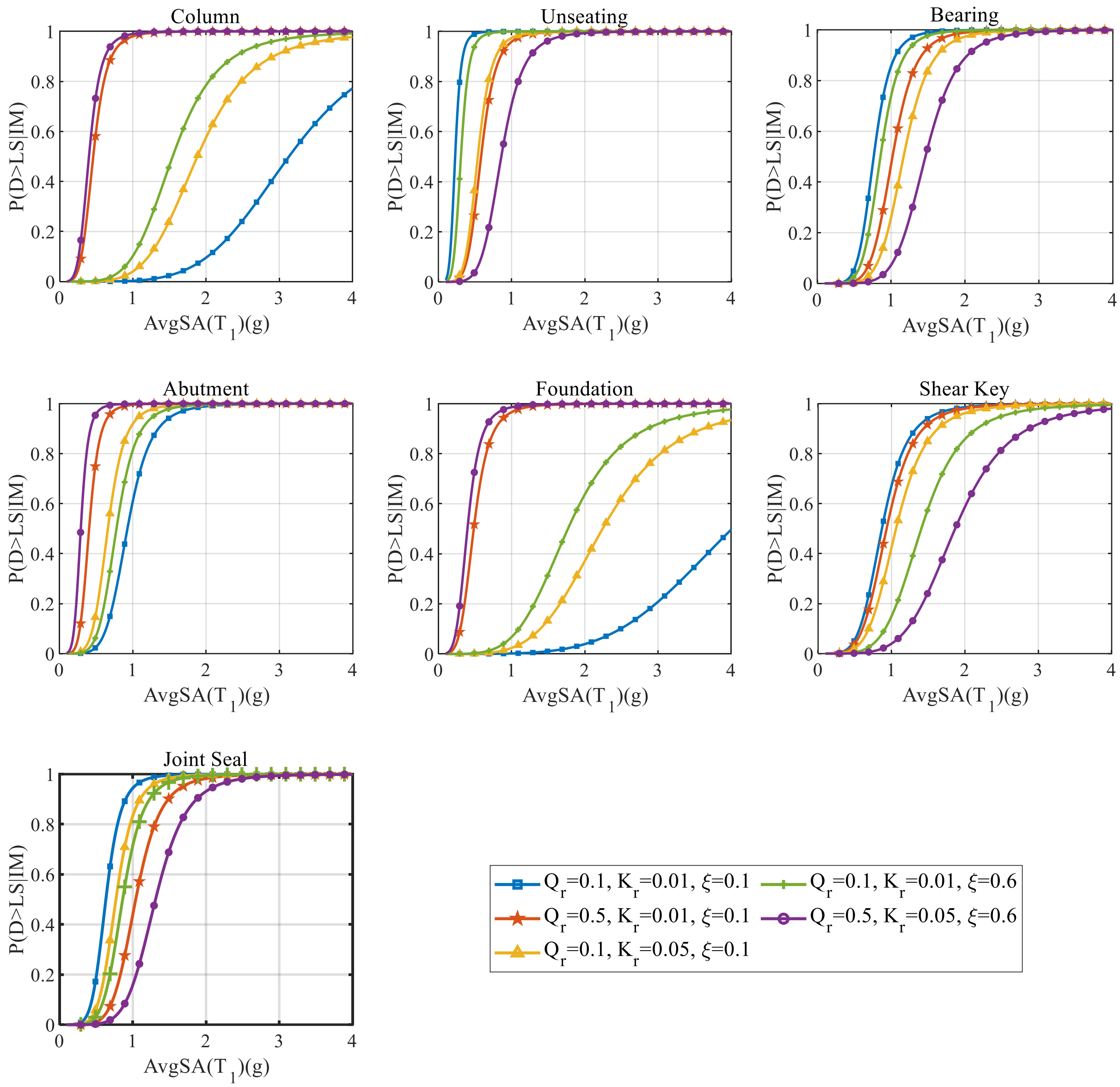

Figure 4.6. Parameterized fragility models for the FPS plus damper case under slight damage state: (a) column; (b) unseating; (c) bearing; (d) abutment; (e) foundation; (f) shear key; and (g) joint seal

foundation, while bridge unseating, bearing, shear key, and joint seal exhibit a reversed trend with decreased seismic fragilities. It is evident that increasing the stiffness and strength of the LRBs would strengthen the connectivity between the bridge superstructure and substructure. As such, seismic fragilities of the substructure components (i.e., column, abutment, and foundation) are increased because of the larger transmitted inertia forces. Conversely, stronger LRBs can reduce the seismic vulnerability of deck unseating and joint seal, as well as the connectivity components such as bearing and shear key. Fig. 4.5 proves the effectiveness of the parameterized fragility models in capturing a reliable and stable seismic fragility for each bridge component, while the associated fragility redistribution across bridge components further calls for risk-based optimization of LRBs at the system level.

Moreover, Fig. 4.6 presents another set of parameterized fragility models for the bridge installed with FPS and viscous dampers and subjected to the slight damage state. Five different design cases are considered by changing not only the stiffness and strength parameters of the bearings, but also the damping ratio provided by the viscous dampers. A consistent conflicting trend of the component fragilities can be observed under these five cases. Namely, the seismic fragilities of substructure components, such as column, abutment, and foundation, would increase when stiffer bearings and larger damper forces are applied to connect them to the superstructure. In contrast, the stronger connectivity would decrease the seismic fragilities of the remaining components, including bridge unseating, bearing, shear key, and joint seal. To this end, the optimal design parameters of isolation bearings and viscous dampers need to be identified to bear a proper trade-off in the seismic fragilities of all bridge components, and one viable strategy is to examine and minimize the seismic risk of the bridge at the system level.

4.6 Damage ratios and replacement costs

As indicated in Eqs. (3.5) and (3.6), the component-level parameterized fragility models are further combined with the seismic hazard model and bridge exposure information to derive the system-level ARCR. The seismic hazard at the bridge site is shown in Fig. 4.3, while the exposure information of the benchmark bridge is tabulated in Table 4.4. In particular, the damage ratio defines the fraction of repair cost at each damage state versus the total replacement cost of one bridge component, while the replacement costs of different components are provided in terms of the percentages of the total bridge construction cost. In this study, possible repair actions at each damage state and their associated material expenditures and unit costs of materials are utilized to compute damage ratios and replacement costs (Sobanjo *et al.*, 2001; Padgett, 2007; Ghosh and Padgett, 2011; Xie and Zhang, 2017). For example, the replacement cost of the bridge column is comprised of the costs from concrete and steel reinforcement, formwork, and paint and coat, etc. (Ghosh and Padgett, 2011). In addition, the replacement cost of the abutment also includes the underneath pile foundation.

Table 4.4. Damage ratios and replacement costs of different bridge components

Component	EDP (*unit*)	Damage ratio				Replacement cost
		S	M	E	C	
Column	Drift ductility	0.03	0.08	0.25	1.00	42.0%
Unseating	Displacement (*mm*)	0.25	1.00	-	-	24.6%
Bearing	Shear strain	0.06	0.15	0.60	1.00	7.9%
Abutment	Displacement (*mm*)	0.08	0.25	1.00	-	16.5%
Foundation	Rotation (*rad*)	0.13	1.00	-	-	7.2%
Shear key	Displacement (*mm*)	0.50	1.00	-	-	0.5%
Joint seal	Displacement (*mm*)	0.50	1.00	-	-	1.3%

For the three design cases that involve fluid viscous dampers, the extra costs of installing the dampers need to be included in the computation of ARCR. Gidaris and Taflanidis (2015) investigated the price of commercially-available dampers and approximated a cost equation through curve fitting. As shown in Eq. (4.5), the damper cost is considered to be dependent on its maximum force capacity:

$$c_{d,i}(\$) = 96.88 \cdot \left(F_{d,max}(kN)\right)^{0.607} \quad (4.4)$$

where $c_{d,i}$ is the cost of the i^{th} damper, and $F_{d,max}$ is the damper force capacity that is estimated based on Eq. (2.2) by (1) observing that the maximum damper velocity in the NLTHAs is around 0.74 m/s, and (2) assuming a safety factor of two. By further using $\Sigma C_{\alpha} = 2m\bar{\omega}\xi$ and combining Eqs. (2.2) and (4.4), the total damper cost can be related to the damping ratio it provides to the bridge system:

$$c_{d,t}(\$) = 22315.9 \cdot \xi^{0.607} \tag{4.5}$$

where $c_{d,t}$ is the total damper cost. It is worth noting that Eq. (4.5) is dependent on the mass and natural period of the bridge structure. In this respect, an extra cost ratio is defined to update the ARCR such that the additional upfront cost of installing viscous dampers can be incorporated into the overall optimization process:

$$ARCR_{damp}(X) = ARCR(X) \cdot \left(1 + \frac{c_{d,t}}{\sum_m c_m}\right) \tag{4.6}$$

The $ARCR_{damp}(X)$ in Eq. (4.6) turns out to be an equivalent ARCR for retrofitting the benchmark bridge when engaging viscous dampers. In essence, it adds a constraint to prevent unrealistic design scenarios of installing too many dampers (i.e., keep increasing ξ) without recognizing the induced extra cost.

4.7 Parameterized ARCR and optimal designs

The computational cost of the overall analysis process took about 36 hours, where the majority of the time has been spent on the nonlinear time history analyses of the bridge when installed with different sets of seismic protective devices. Fig. 4.7 presents the parameterized ARCR surfaces and the associated design contours for the benchmark bridge installed with three types of bearings, respectively. A general observation of Fig. 4.7 concludes that ARCR becomes a convex function that is contingent on Q_r and K_r, which provides a convenient way to visually identify the global

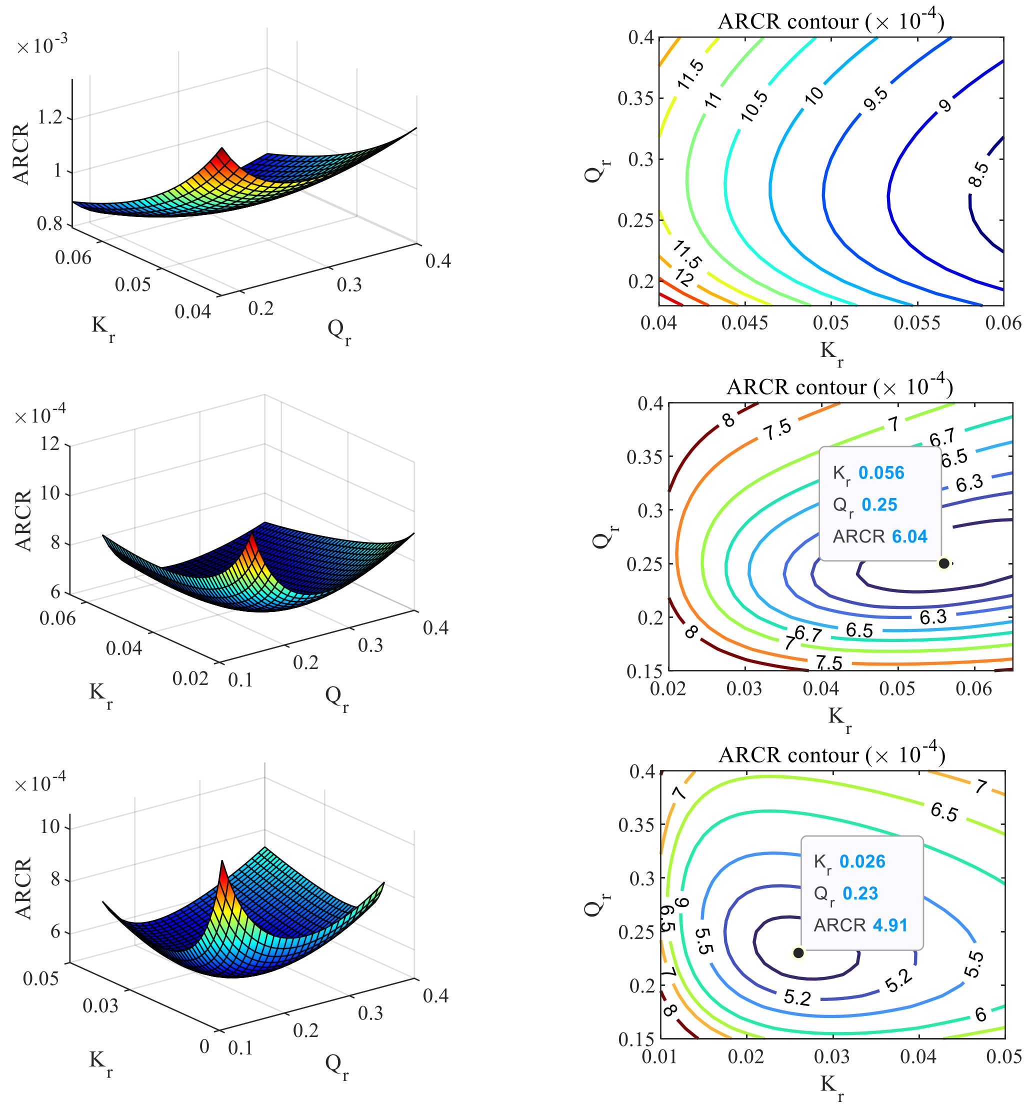

Figure 4.7. Parameterized ARCR surfaces and design contours for the three bearing cases: (a) ERB; (b) LRB; and (c) FPS

minimum and its associated optimal values for Q_r and K_r. In particular, the ARCR of the bridge installed with ERBs (Fig. 4.7(a)) stays in the range between 8×10^{-4} and 1.2×10^{-3}, while the minimal ARCR occurs when Q_r is around 0.25. In this case, the ARCR decreases monotonically when K_r is increasing, which pushes the 'optimal' design value of K_r to be close to its upper

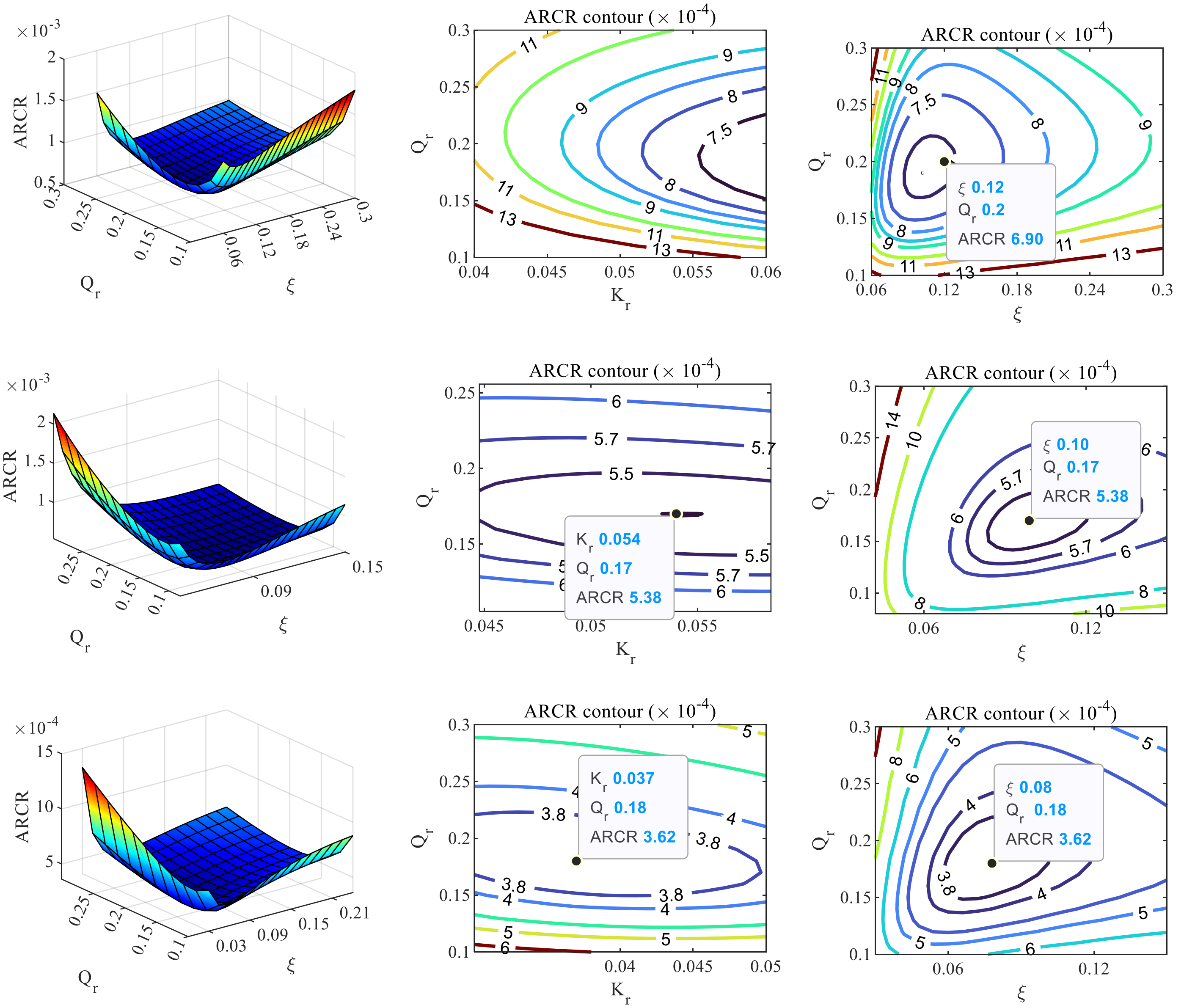

Figure 4.8. Parameterized ARCR surfaces and design contours for the three bearing plus damper cases: (a) ERB + damper; (b) LRB + damper; and (c) FPS + damper

bound. However, this is not the case for the bridge installed with LRBs and FPSs. The ARCR for the LRB case (Fig. 4.7(b)) is well constrained in the range between 6×10^{-4} and 8×10^{-4}, whereas its global minimum can be pinpointed when $Q_r = 0.25$, and $K_r = 0.056$. The FPS exhibits superior effectiveness in mitigating the seismic risk of the benchmark bridge, where the

ARCR in Fig. 4.7(c) is further reduced to the range of $5 \times 10^{-4} - 7 \times 10^{-4}$. In this case, the minimal ARCR of 5×10^{-4} appears when $Q_r = 0.23$, and $K_r = 0.026$.

In addition, Fig. 4.8 presents the parameterized ARCR surfaces and the corresponding design contours for the bridge installed with both bearings and viscous dampers. As shown in the figure, the ARCR can be further reduced by equipping the bridge with viscous dampers. Fig. 4.8(a) first indicates that by installing ERBs and viscous dampers, the system ARCR ranges from 7×10^{-4} and 10×10^{-4}, and the associated minimal ARCR happens when $Q_r = 0.20$, and $\xi = 0.12$. Similar to the ERB only case shown in Fig. 4.8(a), the ARCR in Fig. 9(a) also exhibits a monotonically decreasing trend when K_r is increasing. As such, the identified 'optimal' value for K_r is around 0.06. Fig. 4.8(b) presents the ARCR results for the bridge installed with LRBs and viscous dampers. As shown in the figure, the ARCR is further reduced to be around $5.4 \times 10^{-4} - 7 \times 10^{-4}$. Moreover, the ARCR has its global minimum of 5.4×10^{-4} when the protective devices are designed to have $Q_r = 0.17$, $K_r = 0.054$, and $\xi = 0.10$. Likewise, the coupling of FPSs and viscous dampers shows the best protection strategy among the six design cases. As shown in Fig. 4.8(c), the associated ARCR is generally constrained in the range between 3.6×10^{-4} and 7×10^{-4}, whereas the minimal ARCR of 3.6×10^{-4} appears when $Q_r = 0.18$, $K_r = 0.037$, and $\xi = 0.08$.

Finally, the optimal design parameters of seismic protective devices and the corresponding minimal ARCRs of the benchmark bridge are summarized in Table 4.5. Some general trends can be observed by checking the listed values in the table. First, the optimal design value for the bearing strength stays stable – no matter which bearing type is considered, the optimal Q_r stays around 0.23-0.25 for the bearing only cases, and 0.17-0.20 for the bearing plus damper cases. Conversely, the bearing type would influence the identified optimal values for K_r. A significantly reduced K_r can be identified when FPS is adopted to fully isolated the bridge. The relatively invariant trend occurs regarding the optimal damper design, where the overall optimal damping ratio stays around 0.08-0.12, indicating an optimal damping coefficient C_α = 140.5-210.7 kN (s/m) for dampers at each location (i.e., column top or end abutment). It is worth mentioning that this study recommends using a relatively smaller size of viscous dampers when compared with previous studies (Xie and Zhang, 2017; Xie and Zhang, 2018). Such a difference results from the integration of damper costs in the overall optimization process (i.e., through Eq(15)), which prevents constantly increasing the damper size without taking into account the associated extra cost. The last column in Table 4.5 compares the computed ARCR for the six design cases. It should be noted that the as-built bridge yields an ARCR of around 8.72%, which is due to the fact that many existing bridge components would experience substantial damage when subjected to medium-level earthquake loading. However, such a large ARCR can be significantly reduced when the bridge is fully isolated and installed with supplemental viscous dampers. The optimal ARCR values for the retrofitted bridge stay in the range between 8×10^{-4} and3.62×10^{-4}. Among the three types of bearings, the FPS shows the most outstanding performance in minimizing the ARCR. More importantly, despite the extra cost of installing viscous dampers, combing bearings with viscous dampers can further reduce the ARCR of the bridge, which indeed proves the economic benefits of considering the combined use of isolation bearings and viscous dampers to mitigate the seismic risk of bridge structures. By further comparing the computed ARCR values among these six different design scenarios, one can identify that the optimal design of FPS is the second-best solution in terms of minimizing the seismic risk of the bridge. Therefore, using optimized FPS alone can be a promising strategy in practice, given that the construction complexity of installing the additional viscous dampers can be completely avoided.

Table 4.5. Optimal Designs of Seismic Protective Devices and their associated ARCR

Design Cases	$Q_r = Q/Q_c$	$K_r = K_2/K_{1.c}$	$C_\alpha\ [kN(s/m)]$	$\xi = \frac{\Sigma C_\alpha}{2m\omega_n}$	ARCR ($\times 10^{-4}$)
ERB	0.25	0.060	-	-	8.00
LRB	0.25	0.056	-	-	6.04
FPS	0.23	0.026	-	-	4.91
ERB + damper	0.20	0.060	210.7	0.12	6.90
LRB + damper	0.17	0.054	175.6	0.10	5.38
FPS + damper	0.18	0.037	140.5	0.08	3.62

4.8 Sensitivity analysis

The parameterized ARCR model is developed under a given set of numerical values that define bridge components' capacity models in Table 4.3, as well as their damage ratios and replacement costs in Table 4.4. A sensitivity analysis is further carried out in this study to examine how these values would change the ARCR surface and the associated optimal device design. Due to limited space, this section only discusses the results for the case when LRBs are installed on the bridge, while similar trends can be observed for other design case scenarios. The sensitivity analysis is conducted through the one-at-a-time method (Daniel, 1973), which varies one parameter at a time and keeps the other parameters at their baseline values. In particular, each parameter in Tables 4.3 and 4.4 is changed by plus/minus one dispersion from its median value. The dispersions for the capacity models are listed in Table 4.3, while 0.25 is assumed as the dispersion for damage ratios and replacement costs shown in Table 4.4.

The normalized tornado diagrams are provided in Fig. 4.9 to show the sensitivity of the optimal K_r and Q_r, as well as the minimum *ARCR*, to each changing parameter. Fig. 4.9(a) indicates that the optimal stiffness parameter K_r remains relatively insensitive: its largest variation occurs at 13.0% when a different capacity model is used for bridge abutments. The column's capacity model is the other influential parameter that changes K_r by 10.9%. By contrast, larger sensitivity is observed with respect to the optimal Q_r, which varies between 15% to 25% when a different capacity model is used for bridge column or deck unseating. The capacity models of these two components also bear substantial influences on the minimum ARCR, where a value change of 15-30% is noticed. On the other hand, Figs. 4.9(b) and 4.9(c) indicate that the optimization results are stable when different values are considered for damage ratios and replacement costs. These two figures indicate that the variations in the optimal K_r, Q_r and the minimum ARCR stay within 12%. This is understandable since damage ratio and replacement cost are merely involved in the ARCR model but not the fragility model, which is not the case where capacity models also affect bridge fragility curves. To this end, it is essential to ensure accurate capacity models for bridge column, deck unseating, and end abutments, as these models would substantially influence the final optimization results.

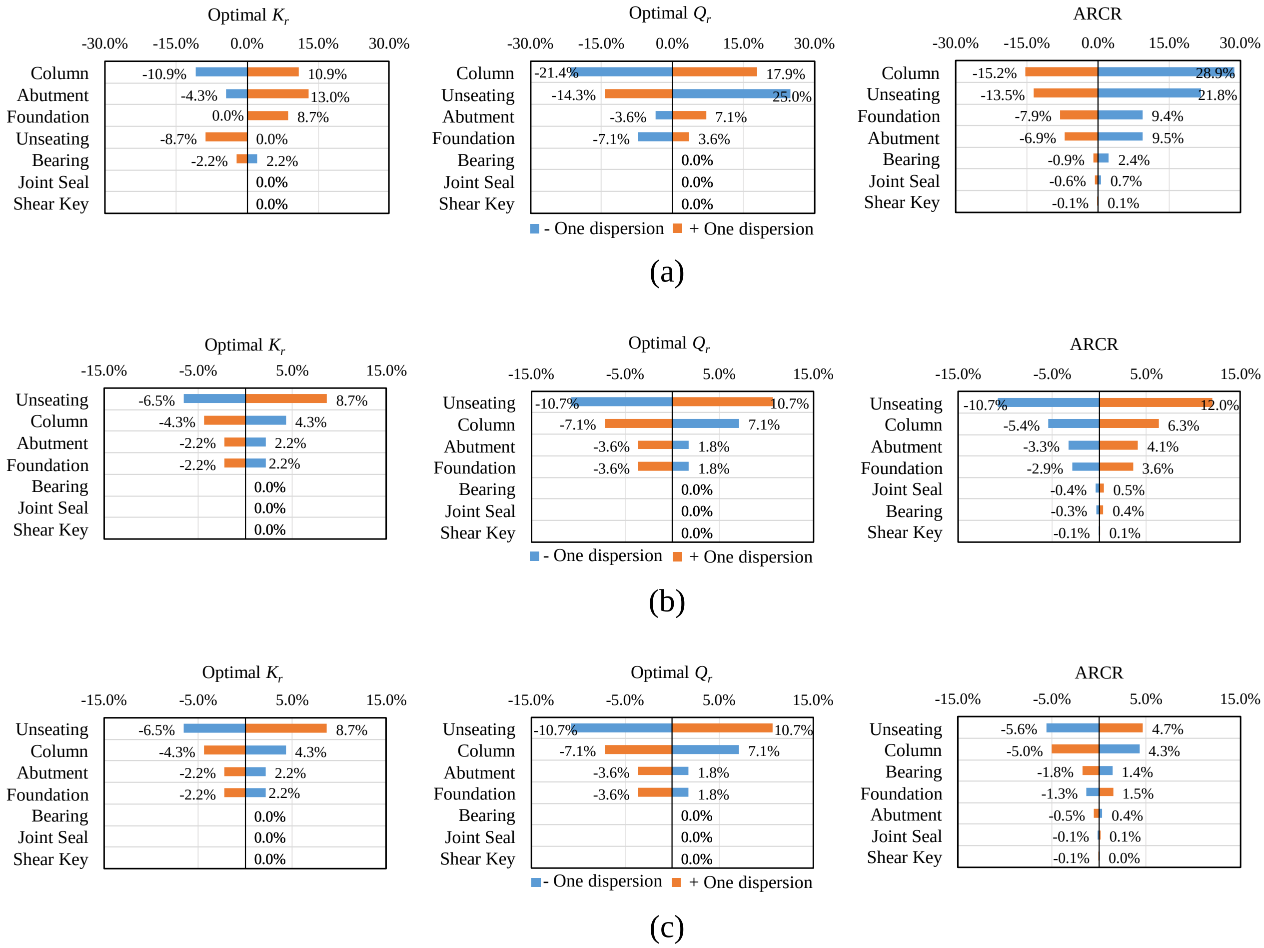

Figure 4.9. Sensitivity of the optimal Kr, Qr, and minimum ARCR for the LRB case when subjected to changing (a) capacity limit state models; (b) damage ratios; and (c) replacement costs

Chapter 5 - Conclusions

The PBEE methodology has been extended in this study to develop a complete risk-based optimization framework that directly links the expected ARCR of the bridge system to the design parameters of seismic protective devices. The framework features the integration of (1) a design of experiment to cover a wide selection of design case scenarios; (2) the logistic regression to develop parameterized fragility models for multiple bridge components; and (3) the derivation of the expected ARCR by convolving the seismic hazard model, fragility model, and bridge exposure information. The *IM*-independent ARCR turns out to be a convex function that can be directly visualized to pinpoint its global minimum and the associated optimal designs for isolation bearings and viscous dampers. Moreover, a case study is conducted to retrofit a benchmark highway bridge in California by considering six different design cases (i.e., three bearing cases, and three bearing plus damper cases). Optimization results from the case study validate the soundness of the proposed framework, whereas the following conclusions can be further drawn from this research:

1. The developed parameterized fragility models capture the redistribution of damage probabilities across multiple bridge components. Namely, increasing the stiffness and strength of seismic protective devices would increase the seismic fragilities of substructure components (i.e., column, abutment, and foundation). Yet, it would simultaneously reduce the seismic vulnerabilities of bearing, span unseating, shear key, and joint seal.
2. The installation of optimally designed isolation bearings and dampers can significantly reduce the seismic risk of the benchmark bridge. Among the three types of bearings, the FPS shows the best effectiveness in minimizing the ARCR. Despite the extra cost of

installing viscous dampers, combing bearings with dampers can further reduce the ARCR of the bridge.

3. Some optimal design parameters of protective devices remain insensitive to the choice of bearing type. The optimal yielding strength Q of the bearing is found to be around $0.25Q_c$ when bearings are solely used. If viscous dampers are installed in conjunction with bearings, the bearings' yielding strength can be chosen as $0.18Q_c$, while a 10% additional damping ratio needs to be provided by the viscous dampers to reach the minimum ARCR.

In summary, this study proposes a first-of-its-kind analysis framework to directly engage the seismic risk of the bridge system into the optimization of seismic protective devices. As a step forward versus the performance-based design methodology, the developed framework can be congruously applied to the design and optimization of any other types of structures and devices. It is worth mentioning that the convexity of the developed ARCR model is essential for generating the unique optimal design of the seismic protective device. Nevertheless, the convexity status of the ARCR is generalizable so long as conflicting seismic responses exist among major components in a structure. For instance, installing damper devices in a building frame will reduce the column damage, but it might increase the floor acceleration at the same time. As such, the resultant ARCR model would most likely turn out to be a convex surface where its minimum value occurs when seismic damage of structural and non-structural components achieve a proper balance. Furthermore, the authors have made ongoing efforts to explore more advanced statistical and machine learning techniques, such as the artificial neural network, that can replace the logistic regression in developing the parameterized seismic fragility models.

References

Abdel Raheem, S. E. (2009) ‘Pounding mitigation and unseating prevention at expansion joints of isolated multi-span bridges’, *Engineering Structures*, 31(10), pp. 2345–2356. doi: 10.1016/j.engstruct.2009.05.010.

Agrawal, A. K. *et al.* (2012) ‘Seismic Fragility of Retrofitted Multispan Continuous Steel Bridges in New York’, *Journal of Bridge Engineering*, 17(4), pp. 562–575. doi: 10.1061/(ASCE)BE.1943-5592.0000290.

Agrawal, A. K. and Amjadian, M. (2022) ‘Seismic component devices’, in *Innovative Bridge Design Handbook*. 2nd edn. Elsevier, pp. 637–662. doi: 10.1016/B978-0-12-823550-8.00027-5.

Akkari, M. *et al.* (2015) *Bridge Engineering: Seismic Design, Taylor & Francis Group, LLC*. Edited by W.-F. Chen and L. Duan. London New York Wshington, D.C. Available at: 978-1-4200-3977-1.

American Association of State Highway and Transportation Officials (AASHTO) (2010) *Guide specifications for seismic isolation design*. AASHTO.

Amjadian, M. and Agrawal, A. K. (2016) ‘Rigid-Body Motion of Horizontally Curved Bridges Subjected to Earthquake-Induced Pounding’, *Journal of Bridge Engineering*, 21(12), p. 04016090. doi: 10.1061/(ASCE)BE.1943-5592.0000962.

Ancheta, T. D. *et al.* (2014) ‘NGA-West2 database’, *Earthquake Spectra*, 30(3), pp. 989–1005. doi: 10.1193/070913EQS197M.

Andrawes, B. and DesRoches, R. (2007) ‘Comparison between Shape Memory Alloy Seismic Restrainers and Other Bridge Retrofit Devices’, *Journal of Bridge Engineering*, 12(6), pp. 700–709. doi: 10.1061/(ASCE)1084-0702(2007)12:6(700).

Applied Technology Council (1996a) *ATC-32, Seismic Design Criteria for California Bridges: Provisional Recommendations*. Redwood City, CA.

Applied Technology Council (1996b) *ATC-40, Seismic Evaluation and Retrofit of Concrete Buildings*. Redwood City, CA.

Baker, J. W. (2011) ‘Conditional Mean Spectrum: Tool for Ground-Motion Selection’, *Journal of Structural Engineering*, 137(3), pp. 322–331. doi: 10.1061/(ASCE)ST.1943-541X.0000215.

Baker, J. W. (2015) ‘Introduction to Probabilistic Seismic Hazard Analysis’, *White Paper Version 2.1*, 77 pp.

Baker, J. W. and Cornell, C. A. (2005) ‘A vector-valued ground motion intensity measure consisting of spectral acceleration and epsilon’, *Earthquake Engineering and Structural Dynamics*, 34(10), pp. 1193–1217. doi: 10.1002/eqe.474.

Baker, J. W. and Lee, C. (2018) ‘An Improved Algorithm for Selecting Ground Motions to Match a Conditional Spectrum’, *Journal of Earthquake Engineering*, 22(4), pp. 708–723. doi: 10.1080/13632469.2016.1264334.

Basöz, N. I. *et al.* (1999) 'Statistical Analysis of Bridge Damage Data from the 1994 Northridge, CA, Earthquake', *Earthquake Spectra*, 15(1), pp. 25–54. doi: 10.1193/1.1586027.

Berquist, M. and DePasquale, R. (2020) *Fluid Viscous Dampers: General Guidelines for Engineers Including a Brief History*. North Tonawanda, NY: Taylor deviices inc.

Bessason, B. and Haflidason, E. (2004) 'Recorded and Numerical Strong Motion Response of a Base-Isolated Bridge', *Earthquake Spectra*, 20(2), pp. 309–332. doi: 10.1193/1.1705656.

Bradley, B. A. *et al.* (2007) 'Improved seismic hazard model with application to probabilistic seismic demand analysis', *Earthquake Engineering & Structural Dynamics*, 36(14), pp. 2211–2225. doi: 10.1002/eqe.727.

Bruneau, M., Wilson, J. C. and Tremblay, R. (1996) 'Performance of steel bridges during the 1995 Hyogo-ken Nanbu (Kobe, Japan) earthquake', *Canadian Journal of Civil Engineering*, 23(3), pp. 678–713. doi: 10.1139/l96-883.

California Department of Transportation (Caltrans) (1994) *Initial and Supplementary Bridge Reports for the Northridge Earthquake*. Sacramento, CA: California Department of Transportation, Division of Structures.

Cardone, D. and Perrone, G. (2017) 'Damage and Loss Assessment of Pre-70 RC Frame Buildings with FEMA P-58', *Journal of Earthquake Engineering*, 21(1), pp. 23–61. doi: 10.1080/13632469.2016.1149893.

Chaudhary, M. T. A. *et al.* (2000) 'System Identification of Two Base-Isolated Bridges Using Seismic Records', *Journal of Structural Engineering*, 126(10), pp. 1187–1195. doi: 10.1061/(ASCE)0733-9445(2000)126:10(1187).

Clark, P. W. (1996) *Experimental studies of the ultimate behavior of seismically-isolated structures*. University of California, Berkeley.

Constantinou, M. C. *et al.* (2007) 'Performance of seismic isolation hardware under service and seismic loading', *Technical Rep. No. MCEER-07*, 12.

Cornell, C. A. *et al.* (2002) 'Probabilistic Basis for 2000 SAC Federal Emergency Management Agency Steel Moment Frame Guidelines', *Journal of Structural Engineering*, 128(4), pp. 526–533. doi: 10.1061/(ASCE)0733-9445(2002)128:4(526).

Cornell, C. A. and Krawinkler, H. (2000) 'Progress and Challenges in Seismic Performance Assessment', *PEER Center News*, 3(2).

Cundy, A. L. *et al.* (2003) 'Use of Response Surface Metamodels for Damage Identification of a Simple Nonlinear System', *Key Engineering Materials*, 245–246, pp. 167–174. doi: 10.4028/www.scientific.net/KEM.245-246.167.

Daniel, C. (1973) 'One-at-a-Time Plans', *Journal of the American Statistical Association*, 68(342), pp. 353–360. doi: 10.1080/01621459.1973.10482433.

DesRoches, R. and Delemont, M. (2002) 'Seismic retrofit of simply supported bridges using shape memory alloys', *Engineering Structures*, 24(3), pp. 325–332. doi: 10.1016/S0141-0296(01)00098-0.

Desroches, R. and Smith, B. (2004) 'Shape memory alloys in seismic resistant design and retrofit: a critical review of their potential and limitations', *Journal of Earthquake Engineering*, 8(3), pp. 415–429. doi: 10.1080/13632460409350495.

Dezi, F. *et al.* (2012) 'Soil-structure interaction in the seismic response of an isolated three span motorway overcrossing founded on piles', *Soil Dynamics and Earthquake Engineering*, 41, pp. 151–163. doi: 10.1016/j.soildyn.2012.05.016.

Dion, C. *et al.* (2011) 'Real-time dynamic substructuring testing of viscous seismic protective devices for bridge structures', *Engineering Structures*, 33(12), pp. 3351–3363. doi: 10.1016/j.engstruct.2011.06.021.

Dion, C. *et al.* (2012) 'Real-Time Dynamic Substructuring Testing of a Bridge Equipped with Friction-Based Seismic Isolators', *Journal of Bridge Engineering*, 17(1), pp. 4–14. doi: 10.1061/(ASCE)BE.1943-5592.0000199.

Dolce, M., Cardone, D. and Marnetto, R. (2000) 'Implementation and testing of passive control devices based on shape memory alloys', *Earthquake Engineering and Structural Dynamics*, 29(7), pp. 945–968. doi: 10.1002/1096-9845(200007)29:7<945::AID-EQE958>3.0.CO;2-#.

De Domenico, D., Ricciardi, G. and Takewaki, I. (2019) 'Design strategies of viscous dampers for seismic protection of building structures: A review', *Soil Dynamics and Earthquake Engineering*, 118(December 2018), pp. 144–165. doi: 10.1016/j.soildyn.2018.12.024.

Dukes, J. (2013) *Application of Bridge Specific Fragility Analysis in the Seismic Design Process of Bridges in California*, *Georgia Institute of Technology*. Georgia Institute of Technology.

Eads, L., Miranda, E. and Lignos, D. G. (2015) 'Average spectral acceleration as an intensity measure for collapse risk assessment', *Earthquake Engineering & Structural Dynamics*, 44(12), pp. 2057–2073. doi: 10.1002/eqe.2575.

Ebadi Jamkhaneh, M., Ebrahimi, A. H. and Shokri Amiri, M. (2019) 'Experimental and Numerical Investigation of Steel Moment Resisting Frame with U-Shaped Metallic Yielding Damper', *International Journal of Steel Structures*, 19(3), pp. 806–818. doi: 10.1007/s13296-018-0166-z.

Eurocode 8 (2005) 'design of structures for earthquake resistance–part 2: bridges (EN 1998-2: 2005)', *Comite Europeen de Normalisation, Brussels*.

Federal Emergency Management Agency (FEMA) (1997) *FEMA 273, NEHRP Guidelines for the Seismic Rehabilitation of Buildings*. Washington, DC.

Federal Emergency Management Agency (FEMA) (2000) *FEMA 356, Prestandard and Commentary for the Seismic Rehabilitation of Buildings*. Washington, DC.

Federal Highway Administration (FHWA) (2021) *Bridge Condition by Highway System*. Washington, DC. Available at: https://www.fhwa.dot.gov/bridge/nbi/no10/condition21.xlsx.

FEMA (2021) *Hazus -MH 2.1 Advanced Engineering Building Module (AEBM)*. Washington, DC: Federal Emergency Management Agency.

Filippou, F. C., Popov, E. P. and Bertero, V. V. (1983) 'Effects of bond deterioration on hysteretic behavior of reinforced concrete joint', *Earthquake Engineering Research Center, University of California, Berkeley*, (August), p. 212.

Floren, A. and Mohammadi, J. (2001) ‘Performance-Based Design Approach in Seismic Analysis of Bridges’, *Journal of Bridge Engineering*, 6(1), pp. 37–45. doi: 10.1061/(ASCE)1084-0702(2001)6:1(37).

Gardoni, P., Mosalam, K. M. and Kiureghian, A. Der (2003) ‘Probabilistic seismic demand models and fragility estimates for RC bridges’, *Journal of Earthquake Engineering*, 7(sup001), pp. 79–106. doi: 10.1080/13632460309350474.

Gerstenberger, M. C. *et al.* (2020) ‘Probabilistic Seismic Hazard Analysis at Regional and National Scales: State of the Art and Future Challenges’, *Reviews of Geophysics*, 58(2), pp. 1–49. doi: 10.1029/2019RG000653.

Ghosh, G., Singh, Y. and Thakkar, S. K. (2011) ‘Seismic response of a continuous bridge with bearing protection devices’, *Engineering Structures*, 33(4), pp. 1149–1156. doi: 10.1016/j.engstruct.2010.12.033.

Ghosh, J. *et al.* (2014) ‘Seismic Reliability Assessment of Aging Highway Bridge Networks with Field Instrumentation Data and Correlated Failures, I: Methodology’, *Earthquake Spectra*, 30(2), pp. 795–817. doi: 10.1193/040512EQS155M.

Ghosh, J. and Padgett, J. E. (2011) ‘Probabilistic seismic loss assessment of aging bridges using a component-level cost estimation approach’, *Earthquake Engineering & Structural Dynamics*, 40(15), pp. 1743–1761. doi: 10.1002/eqe.1114.

Ghosh, J., Padgett, J. E. and Dueñas-Osorio, L. (2013) ‘Surrogate modeling and failure surface visualization for efficient seismic vulnerability assessment of highway bridges’, *Probabilistic Engineering Mechanics*, 34, pp. 189–199. doi: 10.1016/j.probengmech.2013.09.003.

Gidaris, I. and Taflanidis, A. A. (2015) ‘Performance assessment and optimization of fluid viscous dampers through life-cycle cost criteria and comparison to alternative design approaches’, *Bulletin of Earthquake Engineering*, 13(4), pp. 1003–1028. doi: 10.1007/s10518-014-9646-5.

Goda, K. and Atkinson, G. M. (2011) ‘Seismic performance of wood-frame houses in south-western British Columbia’, *Earthquake Engineering & Structural Dynamics*, 40(8), pp. 903–924. doi: 10.1002/eqe.1068.

Goda, K. and Tesfamariam, S. (2019) ‘Financial risk evaluation of non-ductile reinforced concrete buildings in eastern and western Canada’, *International Journal of Disaster Risk Reduction*, 33(September 2018), pp. 94–107. doi: 10.1016/j.ijdrr.2018.09.013.

Goulet, C. *et al.* (2006) ‘Evaluation of the seismic performance of a code-conforming reinforced-concrete frame building - Part I: Ground motion selection and structural collapse simulation’, in *8th US National Conference on Earthquake Engineering*.

Gulerce, Z. *et al.* (2012) ‘Seismic demand models for probabilistic risk analysis of near fault vertical ground motion effects on ordinary highway bridges’, *Earthquake Engineering & Structural Dynamics*, 41(2), pp. 159–175. doi: 10.1002/eqe.1123.

Günay, S. and Mosalam, K. M. (2013) ‘PEER Performance-Based Earthquake Engineering Methodology, Revisited’, *Journal of Earthquake Engineering*, 17(6), pp. 829–858. doi: 10.1080/13632469.2013.787377.

Gur, S., Xie, Y. and DesRoches, R. (2019) 'Seismic fragility analyses of steel building frames installed with superelastic shape memory alloy dampers: Comparison with yielding dampers', *Journal of Intelligent Material Systems and Structures*, 30(18–19), pp. 2670–2687. doi: 10.1177/1045389X19873408.

He, W.-L. and Agrawal, A. K. (2008) 'Analytical Model of Ground Motion Pulses for the Design and Assessment of Seismic Protective Systems', *Journal of Structural Engineering*, 134(7), pp. 1177–1188. doi: 10.1061/(ASCE)0733-9445(2008)134:7(1177).

He, W. *et al.* (2020) 'The influence of pier height on the seismic isolation effectiveness of friction pendulum bearing for Double-Track railway bridges', *Structures*, 28(September), pp. 1870–1884. doi: 10.1016/j.istruc.2020.10.022.

Hu, J. (2014) 'Response of Seismically Isolated Steel Frame Buildings with Sustainable Lead-Rubber Bearing (LRB) Isolator Devices Subjected to Near-Fault (NF) Ground Motions', *Sustainability*, 7(1), pp. 111–137. doi: 10.3390/su7010111.

Jangid, R. S. (2005) 'Optimum friction pendulum system for near-fault motions', *Engineering Structures*, 27(3), pp. 349–359. doi: 10.1016/j.engstruct.2004.09.013.

Javanmardi, A. *et al.* (2020a) 'State-of-the-Art Review of Metallic Dampers: Testing, Development and Implementation', *Archives of Computational Methods in Engineering*, 27(2), pp. 455–478. doi: 10.1007/s11831-019-09329-9.

Javanmardi, A. *et al.* (2020b) 'State-of-the-Art Review of Metallic Dampers: Testing, Development and Implementation', *Archives of Computational Methods in Engineering*, 27(2), pp. 455–478. doi: 10.1007/s11831-019-09329-9.

Johnson, R. *et al.* (2008) 'Large scale testing of nitinol shape memory alloy devices for retrofitting of bridges', *Smart Materials and Structures*, 17(3), p. 035018. doi: 10.1088/0964-1726/17/3/035018.

Kameshwar, S. and Padgett, J. E. (2014) 'Multi-hazard risk assessment of highway bridges subjected to earthquake and hurricane hazards', *Engineering Structures*, 78, pp. 154–166. doi: 10.1016/j.engstruct.2014.05.016.

Karalar, M., Padgett, J. E. and Dicleli, M. (2012) 'Parametric analysis of optimum isolator properties for bridges susceptible to near-fault ground motions', *Engineering Structures*, 40, pp. 276–287. doi: 10.1016/j.engstruct.2012.02.023.

Karim, K. R. and Yamazaki, F. (2007) 'Effect of isolation on fragility curves of highway bridges based on simplified approach', *Soil Dynamics and Earthquake Engineering*, 27(5), pp. 414–426. doi: 10.1016/j.soildyn.2006.10.006.

Kiris, S. S. and Boduroglu, M. H. (2013) 'Earthquake parameters affecting the performance of an RC frame with friction damper', *Soil Dynamics and Earthquake Engineering*, 55, pp. 148–160. doi: 10.1016/j.soildyn.2013.09.007.

Kiureghian, A. Der (2005) 'Non-ergodicity and PEER's framework formula', *Earthquake Engineering & Structural Dynamics*, 34(13), pp. 1643–1652. doi: 10.1002/eqe.504.

Kohrangi, M. *et al.* (2017) 'Conditional spectrum-based ground motion record selection using average spectral acceleration', *Earthquake Engineering & Structural Dynamics*, 46(10), pp. 1667–1685. doi: 10.1002/eqe.2876.

Kohrangi, M., Vamvatsikos, D. and Bazzurro, P. (2017) 'Site dependence and record selection schemes for building fragility and regional loss assessment', *Earthquake Engineering & Structural Dynamics*, 46(10), pp. 1625–1643. doi: 10.1002/eqe.2873.

Lee, D. H. *et al.* (2021) 'Experimental evaluation on the seismic performance of reinforced concrete bridge columns with high strength reinforcement', *Structure and Infrastructure Engineering*, 0(0), pp. 1–11. doi: 10.1080/15732479.2021.1925701.

Lee, D. and Taylor, D. P. (2001) 'Viscous damper development and future trends', *The Structural Design of Tall Buildings*, 10(5), pp. 311–320. doi: 10.1002/tal.188.

Li, H., Liu, M. and Ou, J. (2004) 'Vibration mitigation of a stay cable with one shape memory alloy damper', *Structural Control and Health Monitoring*, 11(1), pp. 21–36. doi: 10.1002/stc.29.

Li, S. *et al.* (2020) 'Seismic vulnerability and loss assessment of an isolated simply-supported highway bridge retrofitted with optimized superelastic shape memory alloy cable restrainers', *Bulletin of Earthquake Engineering*, 18(7), pp. 3285–3316. doi: 10.1007/s10518-020-00812-4.

Losanno, D., Hadad, H. A. and Serino, G. (2017) 'Seismic behavior of isolated bridges with additional damping under far-field and near fault ground motion', *Earthquake and Structures*, 13(2), pp. 119–130. doi: 10.12989/eas.2017.13.2.119.

Luco, N. and Cornell, C. A. (2007) 'Structure-specific scalar intensity measures for near-source and ordinary earthquake ground motions', *Earthquake Spectra*, 23(2), pp. 357–392. doi: 10.1193/1.2723158.

M.D.Symans and M.C.Constantinou (1998) 'Passive fluid viscous damping systems for seismic energy dissipation', *ISET Journal of Earthquake Technology*, 35(December), pp. 185–206.

Mackie, K. R. and Stojadinović, B. (2007) 'Performance-based seismic bridge design for damage and loss limit states', *Earthquake Engineering & Structural Dynamics*, 36(13), pp. 1953–1971. doi: 10.1002/eqe.699.

Mackie, K. R., Wong, J.-M. and Stojadinović, B. (2009) 'Post-earthquake bridge repair cost and repair time estimation methodology', *Earthquake Engineering & Structural Dynamics*, (056), p. n/a-n/a. doi: 10.1002/eqe.942.

Madhekar, S. N. and Jangid, R. S. (2009) 'Variable dampers for earthquake protection of benchmark highway bridges', *Smart Materials and Structures*, 18(11), p. 115011. doi: 10.1088/0964-1726/18/11/115011.

Makris, N. and Zhang, J. (2004a) 'Seismic Response Analysis of a Highway Overcrossing Equipped with Elastomeric Bearings and Fluid Dampers', *Journal of Structural Engineering*, 130(6), pp. 830–845. doi: 10.1061/(ASCE)0733-9445(2004)130:6(830).

Makris, N. and Zhang, J. (2004b) 'Seismic Response Analysis of a Highway Overcrossing Equipped with Elastomeric Bearings and Fluid Dampers', *Journal of Structural Engineering*, 130(6), pp. 830–845. doi: 10.1061/(ASCE)0733-9445(2004)130:6(830).

Mangalathu, S. *et al.* (2016) 'ANCOVA-based grouping of bridge classes for seismic fragility assessment', *Engineering Structures*, 123, pp. 379–394. doi: 10.1016/j.engstruct.2016.05.054.

Mangalathu, S. *et al.* (2017) 'Performance-based grouping methods of bridge classes for regional seismic risk assessment: Application of ANOVA, ANCOVA, and non-parametric approaches', *Earthquake Engineering & Structural Dynamics*, 46(14), pp. 2587–2602. doi: 10.1002/eqe.2919.

Mangalathu, S. (2017) *Performance Based Grouping and Fragility Analysis of Box-Girder Bridges in California*. Georgia Institute of Technology.

Mckay, M. D., Beckman, R. J. and Conover, W. J. (2000) 'A Comparison of Three Methods for Selecting Values of Input Variables in the Analysis of Output From a Computer Code', *Technometrics*, 42(1), pp. 55–61. doi: 10.1080/00401706.2000.10485979.

McKenna, F. (2011) 'OpenSees: A framework for earthquake engineering simulation', *Computing in Science and Engineering*, 13(4). doi: 10.1109/MCSE.2011.66.

Mitchell, D. *et al.* (1995) 'Performance of bridges in the 1994 Northridge earthquake', *Canadian Journal of Civil Engineering*, 22(2), pp. 415–427. doi: 10.1139/l95-050.

Mitchell, D., Tinawi, R. and Sexsmith, R. G. (1991) 'Performance of bridges in the 1989 Loma Prieta earthquake - lessons for Canadian designers', *Canadian Journal of Civil Engineering*, 18(4), pp. 711–734. doi: 10.1139/l91-085.

Mitrani-Reiser, J. *et al.* (2006) 'Evaluation of the seismic performance of a code-conforming reinforced-concrete frame building - Part II: Loss estimation', in *8th US National Conference on Earthquake Engineering*. San Francisco, CA.

Mitrani-Reiser, J. (2007) 'An ounce of prevention: probabilistic loss estimation for performance-based earthquake engineering'. California Institute of Technology.

Mitseas, I. P., Kougioumtzoglou, I. A. and Beer, M. (2016) 'An approximate stochastic dynamics approach for nonlinear structural system performance-based multi-objective optimum design', *Structural Safety*, 60, pp. 67–76. doi: 10.1016/j.strusafe.2016.01.003.

Moehle, J. and Deierlein, G. G. (2004) 'A framework methodology for performance-based earthquake engineering', in *13th world conference on earthquake engineering*. WCEE Vancouver.

Montazeri, M., Ghodrati Amiri, G. and Namiranian, P. (2021) 'Seismic fragility and cost-benefit analysis of a conventional bridge with retrofit implements', *Soil Dynamics and Earthquake Engineering*, 141(November 2020), p. 106456. doi: 10.1016/j.soildyn.2020.106456.

Moreschi, L. M. and Singh, M. P. (2003) 'Design of yielding metallic and friction dampers for optimal seismic performance', *Earthquake Engineering & Structural Dynamics*, 32(8), pp. 1291–1311. doi: 10.1002/eqe.275.

Moridani, K. K. and Zarfam, P. (2013) 'Nonlinear Analysis of Reinforced Concrete Joints with Bond-Slip Effect Consideration in OpenSees', 3(6), pp. 362–367.

Mosalam, K. M. *et al.* (2018) 'Performance-based engineering and multi-criteria decision analysis for sustainable and resilient building design', *Structural Safety*, 74(April), pp. 1–13. doi: 10.1016/j.strusafe.2018.03.005.

Mullins, L. (1969) 'Softening of rubber by deformation', *Rubber chemistry and technology*, 42(1), pp. 339–362.

Muthukumar, S. and DesRoches, R. (2006) 'A Hertz contact model with non-linear damping for pounding simulation', *Earthquake Engineering and Structural Dynamics*, 35(7). doi: 10.1002/eqe.557.

Naeim, F. and Kelly, J. M. (1999) *Design of seismic isolated structures: from theory to practice*. New York: Wiley& Sons.

Narkhede, D. I. and Sinha, R. (2014) 'Behavior of nonlinear fluid viscous dampers for control of shock vibrations', *Journal of Sound and Vibration*, 333(1), pp. 80–98. doi: 10.1016/j.jsv.2013.08.041.

Niederreiter, H. (1992) *Random Number Generation and Quasi-Monte Carlo Methods*. Society for Industrial and Applied Mathematics. doi: 10.1137/1.9781611970081.

Nielson, B. G. (2005) *Analytical Fragility Curves for Highway Bridges in Moderate Seismic Zones*. Georgia Institute ofTechnology.

Nordhausen, K. (2009) 'The Elements of Statistical Learning: Data Mining, Inference, and Prediction, Second Edition by Trevor Hastie, Robert Tibshirani, Jerome Friedman', *International Statistical Review*, 77(3), pp. 482–482. doi: 10.1111/j.1751-5823.2009.00095_18.x.

Olmos Navarrete, B. A. *et al.* (2016) 'Influence of RC jacketing on the seismic vulnerability of RC bridges', *Engineering Structures*, 123, pp. 236–246. doi: 10.1016/j.engstruct.2016.05.029.

Ozbulut, O. E. and Hurlebaus, S. (2011a) 'Optimal design of superelastic-friction base isolators for seismic protection of highway bridges against near-field earthquakes', *Earthquake Engineering & Structural Dynamics*, 40(3), pp. 273–291. doi: 10.1002/eqe.1022.

Ozbulut, O. E. and Hurlebaus, S. (2011b) 'Seismic assessment of bridge structures isolated by a shape memory alloy/rubber-based isolation system', *Smart Materials and Structures*, 20(1), p. 015003. doi: 10.1088/0964-1726/20/1/015003.

Padgett, J. E. (2007) *Seismic Vulnerability Assessment of Retrofitted Bridges Using Probabilistic Methods*. Georgia Institute ofTechnology. Available at: http://hdl.handle.net/1853/14469.

Padgett, J. E., Dennemann, K. and Ghosh, J. (2010) 'Risk-based seismic life-cycle cost–benefit (LCC-B) analysis for bridge retrofit assessment', *Structural Safety*, 32(3), pp. 165–173. doi: 10.1016/j.strusafe.2009.10.003.

Padgett, J. E. and DesRoches, R. (2008) 'Methodology for the development of analytical fragility curves for retrofitted bridges', *Earthquake Engineering & Structural Dynamics*, 37(8), pp. 1157–1174. doi: 10.1002/eqe.801.

Padgett, J. E., DesRoches, R. and Ehlinger, R. (2009) 'Experimental response modification of a four-span bridge retrofit with shape memory alloys', *Structural Control and Health*

Monitoring, p. n/a-n/a. doi: 10.1002/stc.351.

Padgett, J. E., Nielson, B. G. and DesRoches, R. (2008) 'Selection of optimal intensity measures in probabilistic seismic demand models of highway bridge portfolios', *Earthquake Engineering & Structural Dynamics*, 37(5), pp. 711–725. doi: 10.1002/eqe.782.

Park, G.-J. (2007) 'Design of experiments', *Analytic Methods for Design Practice*, pp. 309–391.

Park, S. W. *et al.* (2004) 'Simulation of the seismic performance of the Bolu Viaduct subjected to near-fault ground motions', *Earthquake Engineering & Structural Dynamics*, 33(13), pp. 1249–1270. doi: 10.1002/eqe.395.

Pekcan, G., Mander, J. B. and Chen, S. S. (1999) 'Fundamental considerations for the design of non-linear viscous dampers', *Earthquake Engineering & Structural Dynamics*, 28(11), pp. 1405–1425. doi: 10.1002/(SICI)1096-9845(199911)28:11<1405::AID-EQE875>3.0.CO;2-A.

Perrone, D. and Filiatrault, A. (2017) 'Automated seismic design of non-structural elements with building information modelling', *Automation in Construction*, 84(December 2016), pp. 166–175. doi: 10.1016/j.autcon.2017.09.002.

Petrini, F. *et al.* (2020) 'Multi-Hazard Assessment of Bridges in Case of Hazard Chain: State of Play and Application to Vehicle-Pier Collision Followed by Fire', *Frontiers in Built Environment*, 6(September), pp. 1–19. doi: 10.3389/fbuil.2020.580854.

Porter, K. A. (2003) 'An Overview of PEER's Performance-Based Earthquake Engineering Methodology', in *In Proceedings of ninth international conference on applications of statistics and probability in civil engineering*. San Francisco, p. pp.1-8.

Porter, K. A., Beck, J. L. and Shaikhutdinov, R. V. (2002) 'Sensitivity of building loss estimates to major uncertain variables', *Earthquake Spectra*, 18(4), pp. 719–743. doi: 10.1193/1.1516201.

Porter, K., Kennedy, R. and Bachman, R. (2007) 'Creating fragility functions for performance-based earthquake engineering', *Earthquake Spectra*, 23(2), pp. 471–489. doi: 10.1193/1.2720892.

Ramamoorthy, S. K., Gardoni, P. and Bracci, J. M. (2006) 'Probabilistic Demand Models and Fragility Curves for Reinforced Concrete Frames', *Journal of Structural Engineering*, 132(10), pp. 1563–1572. doi: 10.1061/(asce)0733-9445(2006)132:10(1563).

Ramanathan, K. N. (2012) *Next Generation Seismic Fragility Curves for California Bridges Incorporating the Evolution in Seismic Design Philosophy*. Georgia Institute of Technology.

Roussis, P. C. *et al.* (2003) 'Assessment of Performance of Seismic Isolation System of Bolu Viaduct', *Journal of Bridge Engineering*, 8(4), pp. 182–190. doi: 10.1061/(ASCE)1084-0702(2003)8:4(182).

Sato, M. *et al.* (1994) 'Response of on-netoh bridge during Kushiro-Oki earthquake of January 1993', in *Proceedings, 3rd US-Japan Workshop on Earthquake Protective Systems for Bridges," Report NCEER-94-0009, National Center for Earthquake Engineering Research,* *Buffalo, NY*.

Seo, J. and Linzell, D. G. (2012) ‘Horizontally curved steel bridge seismic vulnerability assessment’, *Engineering Structures*, 34, pp. 21–32. doi: 10.1016/j.engstruct.2011.09.008.

Sharabash, A. M. and Andrawes, B. O. (2009) ‘Application of shape memory alloy dampers in the seismic control of cable-stayed bridges’, *Engineering Structures*, 31(2), pp. 607–616. doi: 10.1016/j.engstruct.2008.11.007.

Silva, P. F., Megally, S. and Seible, F. (2009) ‘Seismic Performance of Sacrificial Exterior Shear Keys in Bridge Abutments’, *Earthquake Spectra*, 25(3), pp. 643–664. doi: 10.1193/1.3155405.

Siqueira, G. H. *et al.* (2014) ‘Fragility curves for isolated bridges in eastern Canada using experimental results’, *Engineering Structures*, 74, pp. 311–324. doi: 10.1016/j.engstruct.2014.04.053.

Sobanjo, J. O. *et al.* (2001) *Development of Agency Maintenance , Repair & Rehabilitation (MR&R) Cost Data for Florida’s Bridge Management System*, *Florida State University*. Available at: http://www.pdth.com/images/fdotagcy.pdf.

Soneji, B. B. and Jangid, R. S. (2007) ‘Passive hybrid systems for earthquake protection of cable-stayed bridge’, *Engineering Structures*, 29(1), pp. 57–70. doi: 10.1016/j.engstruct.2006.03.034.

Song, G., Ma, N. and Li, H.-N. (2006) ‘Applications of shape memory alloys in civil structures’, *Engineering Structures*, 28(9), pp. 1266–1274. doi: 10.1016/j.engstruct.2005.12.010.

Structural Engineers Association of California (SEAOC) (1995) ‘Vision 2000, conceptual framework for performance-based seismic design’, in *Recommended lateral force requirements and commentary*. 6th edn. Sacramento, CA, pp. 391–416.

Symans, M. D. *et al.* (2008) ‘Energy Dissipation Systems for Seismic Applications: Current Practice and Recent Developments’, *Journal of Structural Engineering*, 134(1), pp. 3–21. doi: 10.1061/(ASCE)0733-9445(2008)134:1(3).

Taiyari, F., Mazzolani, F. M. and Bagheri, S. (2019) ‘Damage-based optimal design of friction dampers in multistory chevron braced steel frames’, *Soil Dynamics and Earthquake Engineering*, 119, pp. 11–20. doi: 10.1016/j.soildyn.2019.01.004.

Tesfamariam, S. and Goda, K. (2015) ‘Loss estimation for non-ductile reinforced concrete building in Victoria, British Columbia, Canada: effects of mega-thrust M w 9-class subduction earthquakes and aftershocks’, *Earthquake Engineering & Structural Dynamics*, 44(13), pp. 2303–2320. doi: 10.1002/eqe.2585.

Tsopelas, P. *et al.* (1996) ‘Experimental study of bridge seismic sliding isolation systems’, *Engineering Structures*, 18(4), pp. 301–310. doi: 10.1016/0141-0296(95)00147-6.

Tubaldi, E., Barbato, M. and Dall’Asta, A. (2014) ‘Performance-based seismic risk assessment for buildings equipped with linear and nonlinear viscous dampers’, *Engineering Structures*, 78, pp. 90–99. doi: 10.1016/j.engstruct.2014.04.052.

U.S. Geological Survey (2020) *Earthquake lists, maps, and statisticsat.* Available at:

https://earthquake.usgs.gov/hazards/interactive (Accessed: 24 July 2021).

Wang, Y., Chung, L. and Liao, W. (1998) ‘Seismic response analysis of bridges isolated with friction pendulum bearings’, *Earthquake Engineering & Structural Dynamics*, 27(10), pp. 1069–1093. doi: 10.1002/(SICI)1096-9845(199810)27:10<1069::AID-EQE770>3.0.CO;2-S.

Wei, W. *et al.* (2021) ‘Experimental investigation and seismic fragility analysis of isolated highway bridges considering the coupled effects of pier height and elastomeric bearings’, *Engineering Structures*, 233(September 2020), p. 111926. doi: 10.1016/j.engstruct.2021.111926.

Wen, J. *et al.* (2021a) ‘Performance-based seismic design and optimization of damper devices for cable-stayed bridge’, *Engineering Structures*, 237(February), p. 112043. doi: 10.1016/j.engstruct.2021.112043.

Wen, J. *et al.* (2021b) ‘Performance-based seismic design and optimization of damper devices for cable-stayed bridge’, *Engineering Structures*, 237(February), p. 112043. doi: 10.1016/j.engstruct.2021.112043.

Westenenk, B. *et al.* (2019a) ‘Self-Centering Frictional Damper (SCFD)’, *Engineering Structures*, 197(January), p. 109425. doi: 10.1016/j.engstruct.2019.109425.

Westenenk, B. *et al.* (2019b) ‘Self-Centering Frictional Damper (SCFD)’, *Engineering Structures*, 197(January), p. 109425. doi: 10.1016/j.engstruct.2019.109425.

Xiang, N., Alam, M. S. and Li, J. (2019) ‘Yielding Steel Dampers as Restraining Devices to Control Seismic Sliding of Laminated Rubber Bearings for Highway Bridges: Analytical and Experimental Study’, *Journal of Bridge Engineering*, 24(11), p. 04019103. doi: 10.1061/(ASCE)BE.1943-5592.0001487.

Xiang, N. and Li, J. (2020) ‘Utilizing yielding steel dampers to mitigate transverse seismic irregularity of a multispan continuous bridge with unequal height piers’, *Engineering Structures*, 205(December 2019), p. 110056. doi: 10.1016/j.engstruct.2019.110056.

Xiao, Y. *et al.* (2011) ‘Seismic Behavior of CFT Column and Steel Pile Footings’, *Journal of Bridge Engineering*, 16(5), pp. 575–586. doi: 10.1061/(asce)be.1943-5592.0000198.

Xie, Y. *et al.* (2020) ‘The promise of implementing machine learning in earthquake engineering: A state-of-the-art review’, *Earthquake Spectra*, 36(4), pp. 1769–1801. doi: 10.1177/8755293020919419.

Xie, Y. *et al.* (2021) ‘Probabilistic Seismic Response and Capacity Models of Piles for Statewide Bridges in California’, *Journal of Structural Engineering*, 147(9), p. 04021127. doi: 10.1061/(asce)st.1943-541x.0003085.

Xie, Y., Huo, Y. and Zhang, J. (2017) ‘Development and validation of p-y modeling approach for seismic response predictions of highway bridges’, *Earthquake Engineering & Structural Dynamics*, 46(4), pp. 585–604. doi: 10.1002/eqe.2804.

Xie, Y. and Zhang, J. (2017) ‘Optimal Design of Seismic Protective Devices for Highway Bridges Using Performance-Based Methodology and Multiobjective Genetic Optimization’, *Journal of Bridge Engineering*, 22(3), p. 04016129. doi: 10.1061/(ASCE)BE.1943-5592.0001009.

Xie, Y. and Zhang, J. (2018) ‘Design and Optimization of Seismic Isolation and Damping

Devices for Highway Bridges Based on Probabilistic Repair Cost Ratio', *Journal of Structural Engineering*, 144(8), p. 04018125. doi: 10.1061/(asce)st.1943-541x.0002139.

Yoon, Y. H. *et al.* (2019) 'Probabilistic Damage Control Application: Implementation of Performance-Based Earthquake Engineering in Seismic Design of Highway Bridge Columns', *Journal of Bridge Engineering*, 24(7), p. 04019068. doi: 10.1061/(ASCE)BE.1943-5592.0001443.

Zhang, J. and Huo, Y. (2009) 'Evaluating effectiveness and optimum design of isolation devices for highway bridges using the fragility function method', *Engineering Structures*, 31(8), pp. 1648–1660. doi: 10.1016/j.engstruct.2009.02.017.

Zheng, Q. *et al.* (2021) 'Influence of abutment straight backwall fracture on the seismic response of bridges', *Earthquake Engineering and Structural Dynamics*, 50(7), pp. 1824–1844. doi: 10.1002/eqe.3423.

Zhou, L., Wang, X. and Ye, A. (2019) 'Shake table test on transverse steel damper seismic system for long span cable-stayed bridges', *Engineering Structures*, 179(October 2018), pp. 106–119. doi: 10.1016/j.engstruct.2018.10.073.

Zhu, J. *et al.* (2016) 'Seismic Design of a Long-Span Cable-Stayed Bridge with Fluid Viscous Dampers', *Practice Periodical on Structural Design and Construction*, 21(1), p. 04015006. doi: 10.1061/(ASCE)SC.1943-5576.0000262.